UNIVERSITAT POLITÈCNICA DE CATALUNYA
BARCELONATECH
Escola Superior d'Enginyeries Industrial,
Aeroespacial i Audiovisual de Terrassa

Degree:

**Bachelor's Degree in Aerospace Vehicle Engineering**

Student:

**Christian Jané Ippel**

Title:

# STUDY OF FLOW CONTROL MECHANISMS WITH OPENFOAM

Director:

**Martí Coma Company**

Co-directors:

**Josep Maria Bergadà Granyó**

**Jordi Pons Prats**

Delivery date:

**June 2019**

Content:

**Report**

# STUDY OF FLOW CONTROL MECHANISMS WITH OPENFOAM

**Report**

Christian Jané Ippel

Director:
Martí Coma Company
Co-directors:
Josep Maria Bergadà Granyó
Jordi Pons Prats

Bachelor's Degree Thesis

Bachelor's Degree in Aerospace Vehicle Engineering

Escola Superior d'Enginyeries Industrial, Aeroespacial i Audiovisual de Terrassa
Universitat Politècnica de Catalunya

June 2019

# Acknowledgment

I would like to thank the supervisors of my Thesis Martí Coma Company, Jordi Pons Prats and Josep Maria Bergadà Granyó for the support given and the knowledge provided during the development of the study.

Josep Maria Bergadà Granyó has put all his attention and has given the knowledge and material resources at his disposal whenever I required them. I am extremely grateful for all things I have learnt from him.

I appreciate the support of Marti, along with his wise advice for the realization of the study and I thank Jordi for having given me access to the CIMNE cluster. Also to both of them for the opportunity of developing such a innovative research.

# Abstract

The main focus of the study is the implementation of a Zero-Net-Mass-Flux (ZNMF) boundary condition on the airfoil NACA 4415, with the intention of evaluating the effects of an Active Flow Control (AFC) mechanism in the boundary layer and in the airfoil performance. The structure of the current Thesis begins with an introduction on Computational Fluid Dynamics, the definition of an OpenFOAM case and a brief description on periodic forcing Active Flow Control mechanisms, composing the Chapter 1. The Chapter 2 consists in the definition of the geometric and phyisical conditions of the study and overviews the procedure to implement AFC. The description and execution of the computational domain is addressed in Chapter 3 with its respective quality check. Having the finite volume discretization of the domain, the Chapter 4 presents the OpenFOAM set up. A mesh independency test is carried out in Chapter 5 in order to select the proper mesh to follow the study. The results obtained of the Baseline case are analysed in Chapter 6 with the aim of implementing the slot of the ZNMF, afterwards, the AFC parameters are defined and the new mesh and boundary conditions are generated. In Chapter 7 the results are exposed making a comparative study with different inlet velocity configurations. Finally, the conclusions of the Thesis are discussed in Chaper 8 and the future work of the study is presented.

# Contents

# List of Figures

# List of Tables

# Aim

The aim of this Thesis is to develop a Computational Fluid Dynamics study of a Zero-Net-Mass-Flux implementation and to evaluate its effect on the boundary layer. The process is carried out with the distinguished CFD open source software OpenFOAM and the Salome open source platform. The slot boundary condition implementation will be placed on the NACA 4415 airfoil, and its resulting performance will be evaluated. Different momentum coefficients and frequencies on the jet velocity signal will be compared.

# Scope

In this study, an introduction into the Computational Fluid Dynamics is needed in order to develop the study of the influence of active flow control mechanisms. As OpenFOAM is the software used, the methodology to perform simulations will have to be learnt and the possibilities given by OpenFOAM will have to be analysed in order to solve the case of study properly.

With the objective to create the mesh with high control and definition, the geometry and meshing skills with Salome software will have to be acquired, also, a research of the parameters that influence on the quality of a good mesh as the domain dimensions will have to be carried out.

It will be necessary to learn and understand the procedures to perform a validated study in computational simulations by performing a mesh independence test. For this reason, it is needed to acquire skills on mesh generation and be aware of the consequences of the mesh quality, having in to account the accuracy level and the computational cost.

As this study focuses on active flow control, the results from the data solution of the baseline simulations will be needed to interpret in order to place the active flow control properly. Apart from that, it will be needed to fully understand the physics inside the boundary layer to understand the appearance or not of improvements. Parameters that define the active flow control applied are needed to be calculated and set up in OpenFOAM.

As the case of study contemplates several simulations, it demands high computational power and thanks to CIMNE resources, it has been used a cluster to solve the different cases. For this reason, the remote computer access methodology will be learnt.

# Requirements

The main requirement is to implement active flow control into an airfoil and evaluate its results compared with the Baseline case. The problem have to be studied with computational fluid dynamics (CFD).

The CFD study has to be done with OpenFOAM and it has to include a mesh independence test for different sizes and number of cells, in order to verify the results.

Since the problem is by nature transient, it has to be chosen a solver which can evaluate results over time. Moreover, it is needed to chose properly the turbulence model in order to capture as best as possible the effects on the boundary layer.

The scope of the study must meet the resources and knowledge available. Moreover, the study had to be done in four months, in accordance to the time duration of one semester. Therefore, it has to be chosen the proper simplification of the problem in order to accomplish the requirements. For instance, the active flow control will be simulated as a boundary condition, and will not be included the mechanism. The Reynolds number and the presence of turbulence model are needed to be well chosen. It will be possible to approximate the problem into a 2D and treat the fluid as incompressible.

# Justification

The main goal of aerodynamics is to improve the performance of an aircraft. This has been persuaded trying different techniques that increase the lift of the wing while reducing the drag. One of the methods that is currently in development is the Zero-Net-Mass-Flux actuator, which enhance the performance of an airfoil by modifying the behaviour of the fluid in the boundary layer.

The present Thesis is being developed with the International Centre for Numerical Methods in Engineering, which is focused in numerical methods and computational techniques, searching for the newest developments on engineering. This study will be based on the implementation of an Active Flow Control mechanism using OpenFOAM, which could be used in the future as a baseline study for the implementation of these devices.

# Chapter 1

# Introduction

The aim of this Chapter is to introduce the Computational Fluid Dynamics methodology and the definition of an OpenFOAM to be able to follow with the next chapters. Moreover, a brief description on periodic forcing Active Flow Control mechanisms is included and how they influence the performance.

## 1.1 CFD with OpenFOAM

The aim of this section is to introduce the Computational Fluid Dynamics methodology in order to have a first notion of the process that will be carried out during the study. Moreover, an overview of OpenFOAM structure is given.

### 1.1.1 Brief description of CFD

CFD is the analysis of problems involving fluid flow and its associated phenomenons by means of computer-based simulation. It can be explained in three main steps: pre-process, solving and post-process.

The pre-process consist on setting the input values of the problem. This includes the definition of the geometry to be studied and the discretization in finite volumes where fluid will flow, also known as computational domain definition and mesh generation. Moreover, it has to be specified the fluid properties and the conditions of the flow at the boundaries of the computational domain.

Pre-processing is crucial for solving properly a problem with CFD. Since the solution of the fluid will be given at nodes inside the finite volumes, the accuracy of the results will depend on the number of subdivisions. It has to be noted that for better accuracy, there is higher computational cost. Pre-processing can consume about half of the time designated to solve a problem with CFD.

In order to solve a case, it has to be done three steps. The numerical algorithm for solving these kind of problems starts by integrating the governing equations in the domain, to be later on discretize into an algebraic system of equations. Afterwards, the solution of the equations is found by applying an iterative method. The integration of the volumes consist on applying conservation of an specified variable to each finite volume.

The conservation is usually evaluated as a balance: for a given variable $\phi$, it consist on equalizing the rate of change of $\phi$ with respect to the time in the volume, to the rate of increase of $\phi$ due to the transport of fluid flow entering to the volume, plus, the rate of increase of $\phi$ due to the variation of the variable from point to point, plus, the rate of generation of $\phi$ in the volume.

The last step, post-processing, consist on processing the data generated in order to make more understandable the result. This includes the generation of plots, vector fields, streamlines, dynamic displays, etc. for the problem solved.

### 1.1.2 OpenFOAM for solving CFD problems

OpenFOAM, as a C++ library, is used primarily to create executables, known as applications. The applications fall into two categories: solvers, that are each designed to solve a specific problem in continuum mechanics; and utilities, that are designed to perform tasks that involve data manipulation.

### 1.1.3 Creating a case in OpenFOAM

To perform a simulation it must be created a case directory with the following subdirectories and files:

#### 1.1.3.1 Time directory: 0

The time directory, for example named 0 if $t_0 = 0$, contains the boundary and initial conditions for at least all variables that will be used in the calculations.

Initial conditions files:

- file **p**: initial pressure field, units, and boundary conditions.
- file **U**: initial velocity field, units, and boundary conditions.

If the case is turbulent, depending on the turbulence model are needed some variables or others.

#### 1.1.3.2 constant directory

The constant directory contains files that define the mesh as well as files in which the thermophysical and turbulence settings are specified.

- folder **polyMesh**: folder containing the mesh definition.
- file **transportProperties**: physical properties such as viscosity (nu) and density (rho).
- file **turbulenceProperties**: type of turbulence model used.

#### 1.1.3.3 system directory

The system directory contains the files in which the discretization schemes, linear system solvers, parallelisation settings, solver settings and control settings are specified.

- file **controlDict:** controls the solvers behaviour
- file **fvSchemes:** numerical schemes for terms calculated during the simulation (time derivatives, gradients, laplacian, etc)
- file **fvSolution:** algorithms used for solving
- file **decomposeParDict:** separates in subprocesses the domain if the case is wanted to be parallelised.

## 1.2 Active Flow Control

Active flow control has been used for many years to control the boundary layer with the aim of improving aerodynamic performance. Nowadays, it is a field with high interest due to the wide range of applications it has. Actively control the fluid flow can delay the separation point, reduce the drag, improve lift, suppress noise, enhance mixing combustion chambers, etc. and therefore, it can improve performance and comfortably, fuel consumption savings, environmental contamination etc.

As the present Thesis is focused on the influence caused by different configurations of one specific mechanism: zero-net-mass-flux, an specify explanation on the methodologies used to modify the boundary layer thickness and separation points will be given.

By enhancing the friction coefficient of the mean separation region, it is possible to achieve separation delay. The use of constant blowing, suction and periodic forcing, increment the momentum transfer to the near wall, and consequently, increment sufficiently the friction coefficient to achieve separation delay. According to [2], using periodic addition of momentum appears to be more efficient than steady momentum addition, regarding energy needed. Specially when the frequency used is a little above the vortex shedding frequency of the problem, it is possible to save around 90% of momentum required if constant injection were used [2]. Therefore, when applying pulsating flow, it is needed a previous study in order to set a particular frequency and amplitude to be efficient when generating vortexes.

Most common devices to generate periodic forcing are fluidic oscillators and zero-net-mass-flux actuators. Fluidic oscillators lack of moving parts on the mechanisms, therefore, they are more reliable. Nevertheless, ZNMFA devices do not need of a flow supply, and thus, do not require a flow feeding system. Some example of current studies in this field are [3] and [4].

# Chapter 2

# Case Of Study

This chapter defines the geometry and physical conditions of the study presented. Moreover, it is guessed what kind of detachment is expected.

Apart fro that, it overviews the procedure to study active flow control into an airfoil and how it is explained in the current study.

## 2.1 Airfoil geometry and Physical conditions

The study will be carried out over a NACA airfoil, created by National Advisory Committee for Aerodynamics of four digits, NACA 4415. Four digit NACA's airfoils are defined by three parameters indicated in its own name. The first number indicates the maximum camber in percent of the chord and the second where it is located from the leading edge in tenths of the chord. Last two numbers sets the relative thickness, that is to say, maximum thickness of the airfoil in percent of chord. In Figure 2.1 the airfoil is shown.

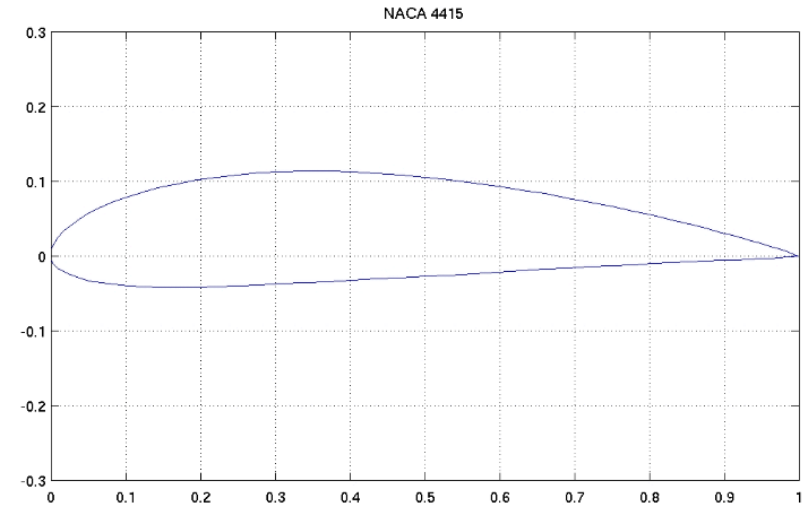


FIGURE 2.1: NACA 4415 coordinates extracted from [1].

The geometry of the case is considered a medium thickness airfoil according to [5], since it has a relative thickness between 0.08 to 0.15.

Medium thickness airfoils are characterized by the appearance of a small bubble before achieving the angle of attack (AoA) of maximum lift coefficient. According to [6], depending on the length of the bubble, lift may decrease and drag increase due to the alterations produced on the pressure distribution. While increasing the AoA, the bubble tends to the leading edge and increase its energy until the flow can not reattach t other airfoil and stall occurs.

The AoA in the current study will be set a $10^{a}$, thus, it will be expected to find the bubble near the leading edge. The airfoil chord will have a length of 0.2m.

Since the purpose of this Thesis is to study an academic problem, it will be carried out at low Reynolds number in order to safe computational time. Therefore, it must be chosen a set of physical properties to develop the study. Table 2.1 summarizes the physical conditions of the case of study.

| | |
|---|---|
| Reynolds number | Re = 6.1 $\times 10^4$ |
| Freestream velocity | $u_\infty$ = 4.5 [m/s] |
| Density | $\rho = 1.225[Kg/m^3]$ |
| Dynamic viscosity | $\mu$ =1.805$\times 10^{-5}$ [kg/ms] |
| Chord | c = 0.2 [m] |
| Angle of attack | AoA = $10^o$ |

TABLE 2.1: Physical conditions.

## 2.2 Resolution of the case

In order to solve the case of the study, it will be first generated different meshes to later develop the mesh independence test (Chapter 5). In order to introduce AFC into the airfoil it first has to be solved the case without AFC, that case is called the Baseline (Chapter 6). With that information, it will be decided where to implement the slot on the AFC (Chapter 6) and finally, the results of AFC cases will be compared (Chapter 7).

In the following part of the subsection, it will be explained how it has been chose turbulence model for solving the case.

### 2.2.1 Turbulence modelling

As explained in the scope of the Thesis, in the current study will not be developed a comparison of the results for different turbulence models. However, it has been chosen with the next criteria.

The current study has been ambitious with the aim, planning to study several cases of AFC. Therefore, it is essential to search for the optimal time of solving cases. Furthermore, the case to study will be based on an aerodynamic geometry. According to [7], the turbulence model Spalart-Allmaras is presented to perform correctly in aerodynamic studies, since it has been created with that purpose.

Moreover, this turbulence model has only one transport equation for the kinematic eddy viscosity parameter, therefore it provides economical computations of boundary layer in external aerodynamics. Apart from that, at the beginning of this section it was mention that the airfoil of study will generate a laminar bubble in extrados. Based on that, it has been found a reference [8] of a study in which the Spalart-Allamaras is successfully evaluated on describing the laminar bubble separation. To sum up, this reference validates the robustness of the approach and assures that the model is able to capture the laminar bubble separation without any external transition mechanism.

In Section 4.2.3, is explained how it has been implemented to OpenFOAM.

# Chapter 3

# Geometry and Mesh

The aim of this Chapter is to define the computational domain. The Chapter will be divided in three sections, following the steps to generate the mesh with Salome 9.2.1; domain geometry, domain discretisation and extrusion. Afterwards, the quality of the mesh is evaluated.

First of all, the geometry of the airfoil is introduced and the domain around the geometry is created with its appropriate size, assuring that the result does not depend on the far field distance. Moreover, the domain is subdivided in regions to mesh each face separately with a higher control and accuracy. Once the domain is defined, it is presented the discretisation used, putting special emphasis on the boundary layer and its cell size and shape requirements, as it is where higher gradients are encountered. Finally, the 2D mesh has been extruded into 3D to generate the finite volumes needed for solving.

Salome 9.2.1 is an open-source software which allows the user build meshes both graphic and coded with a Python console. The Python console is useful to manipulate data before importing it to the mesh and the graphic support let the user check easily and rapidly the state and quality of the mesh. [9]

## 3.1 Domain geometry

Primarily, the airfoil of the case, NACA 4415, has been introduced as a list of points [10] using the Python console in order to speed up the definition of the coordinates. Once the points are placed, a spline can be created with the interpolation tool.

Around the geometry, the domain where the fluid flow will be computed has to be created. It is of high importance to choose a proper computational domain shape, having into account the features of the case. Ideally the size of the domain should be the smallest to achieve less computational cost, as long as the result is independent of the domain size. Apart from that, in the study of aerodynamic shapes it is practical to generate a mesh valid for different AoA.

Since the study is carried in 2D, the geometry of the mesh is defined also in 2D. In two dimensional CFD studies around an airfoil different domain shapes can be used. The most common are the squared, circular and the C-grid domains, represented in the Figure 3.1.

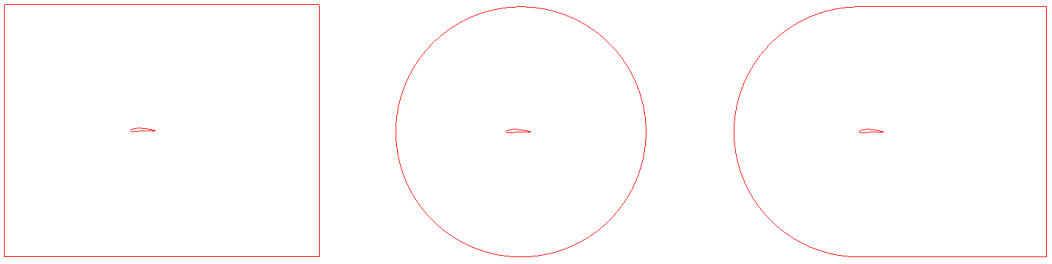

(A) (B) (C)

FIGURE 3.1: Common 2D meshes for airfoil studies (a) Squared, (b) Circular and (a) C-grid.

The boundary conditions of the case demand an inlet, outlet and an airfoil wall, therefore, each edge of the domain has to be classified in one the them. Those three domains presented are not perfectly valid for the case of study. The main reason is due to the uncertain definition of the boundaries if different AoA are wanted to be studied. For instance, the upper and bottom surfaces would act as inlet or outlet depending on the sign of the AoA, positive or negative.

Having stated the previous, a different domain is going to be used which has more consistency. The chosen domain shape is shown in figure 3.2, which is composed by a parabola as an inlet and a vertical line as the outlet.

The parabola is in reality composed by an arc and an inclined line. It has to be noted that the inclination of the edges between the arc and the vertical line sets a maximum value of AoA to simulate, in order to have only the vertical line as the outlet. In this case, this angle is of 20º, since the case of study will not be analyzed for such high AoA.

Once the shape is selected, the size must be discussed. The way to find the proper size is to create different options, simulate them and compare the results in order to find the convergence of the results. In the present case, the dimensions have been extracted from same Reynolds number problem of a PhD researcher in UPC that has already been validated. These dimensions selected are the ones shown in the Figure 3.2, it should be noted that dimensions are expressed with the chord length.

It is important to mention the relation between the Reynolds number and the far field distance. For higher Reynolds number bigger vortex shedding appears, thus, more energy has to be dissipated. The energy of the vortexes is transferred to smaller ones until the size of them reaches the Kolmogorov scale and the lasting energy is dissipated into heat.

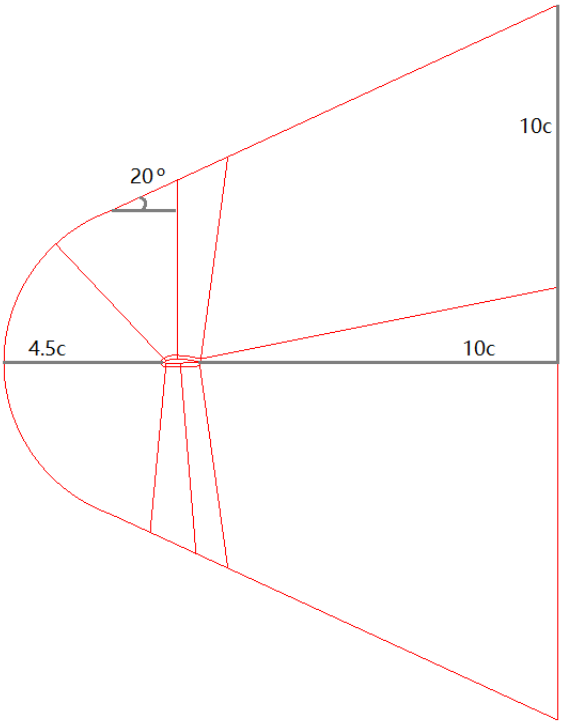


FIGURE 3.2: Domain geometry of the case.

As can be seen on the Figure 3.2, different regions have been created for a better discretisation of the domain, however these regions are mainly due to the boundary layer discratisation, which will be explained next. Also, special attention has been placed in the downstream region where also a finer mesh will be needed.

As exposed in Chapter 1, it is expected to find higher gradients near the airfoil wall and, therefore, it has been included a smaller domain on the boundary layer region. The same procedure has been done in the wake region, in order to capture the vortex shedding. The different faces enable a better control in the discretisation and more accuracy in the result wanted.

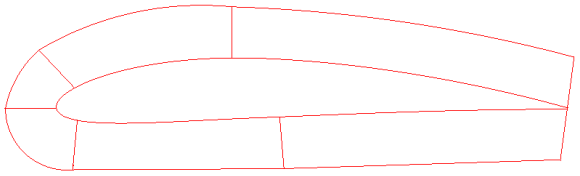

FIGURE 3.3: Boundary layer domain geometry.

## 3.2 Domain discretization

The geometry created is the base from where cells will be created. In order to build this cells, the mesh has to be chosen between structured or unstructured.

Structured meshes are based on quadrilateral elements and can deal with simple geometries. When the geometry becomes more complex it is often used a subdivision of the domain each of which is meshed separately and connected with neighbours. Whereas unstructured meshes can mix triangular and quadrilateral elements allowing the user the generation of mesh around an arbitrary geometry without having to spend that much time. Nowadays it is a common a practice to use in commercial CFD codes automatic generation and semi-automatic mesh refinement.

In the case of study a structured mesh has been chosen not only because it has higher control on the discretisation but also because it can use more efficient algorithms and, thus, it achieves convergence earlier. However, the design and construction of it requires more dedication time.

The methodology carried out has been first, defining each face as a 2D quadrangle mesh and afterwards, each edge from each region has been discretised by selecting the number of segments and the growth rate between them.

### 3.2.1 Boundary layer mesh

As shown in figure 3.3, the boundary layer is meshed separately using its own geometry. The mesh in this region has to be very fine and the parameters that define the cells in this region have to be carefully selected. This parameters are presented in the following sections classified in normal and tangent to the airfoil.

#### 3.2.1.1 Normal discretization

The normal discretization in the boundary layer implies the study of the first cell height ($\Delta y_1$). This length is of major importance in order to guarantee the reliability of the mesh. In such region it is expected to find considerable changes in velocity and pressure, specially in Y-direction as explained in Chapter 1. At this point it is needed to discuss the dimensionless wall height in order to obtain the first cell height. Aditionally, it is needed to evaluate the growing length of the segments and the cell width.

**Dimensionless wall height**

The $y^+$ represents the dimensionless distance from a solid wall taking into account the wall shear stress $\tau_w$, freestream density $\rho$ and kinematic viscosity $\nu$ (or the friction velocity $u_\tau$). This parameter is defined as follows,

$$y^+ = \frac{u_\tau y}{\nu}, \quad u_\tau = \sqrt{\frac{\tau_w}{\rho}} \tag{3.1}$$

With this parameter the boundary layer and mean flow velocity can be studied in three regions depending on shear stress behaviour.

- Viscous sub-layer, $y^+<5$

  In this thin region the fluid is very close to the wall and it is dominated by viscous effects. For this reason, shear stresses might be assumed constant and equal to wall shear stresses. Therefore, it can be found a linear relation between the mean velocity and the distance to the wall because

  $$\tau(u) = \mu\frac{\delta U}{\delta y} \approx \tau_w \quad \Rightarrow \quad U = \frac{\tau_w y}{\mu} \tag{3.2}$$

  Adimensionalising the mean velocity with friction velocity it is obtained $u^+ = y^+$.

- Buffer layer, $5<y^+<30$

  From this $y^+$ range the velocity behaviour can not be defined because of the similar magnitude between wall shear stresses and Reynolds stresses. It is considered the transition region of the shear stress.

- Log-law layer, $y^+>30$

  After the transition region the Reynolds stresses dominate and the shear stress varies slowly with the distance to the wall. In this case it is found a logarithmic relation between $y^+$ and $u^+$,

$$u^+ = \frac{1}{k} ln(y^+) + B \tag{3.3}$$

  where $k$ is von Karman's constant,

  $B$ is an adjustment for wall roughness.

In the light of the above, if the complex flow structure based on fast changes in velocity due to the changing dominance between the viscous effect and Reynolds shear stresses are wanted to be considered, even the viscous sub-layer has to be discretised.

Therefore, velocity and pressure values inside $y^+<5$ are needed, so the first $\Delta y$ of the mesh may be calculated from $y^+<1$ or less. For this reason, in Chapter 5 is presented the mesh convergence for different values of $\Delta y$, with the aim of choosing the one that captures this effects with less computational cost while its results do not change if the mesh gets finer.

**Growth rate**

After defining the first cell height, it has to be set the number of segments along the normal edges of the boundary layer. As it is crucial to save computational cost, it is a practical solution to use an increasing growth rate with the increase of distance from the wall. This is possible since it is expected to find smaller gradients when moving away from the wall, while the number of cells can be reduced considerably.

This growth rate should be small, below 5%, to have a continuous discretisation, not abrupt. It has to be noted that the mesh is different if a DNS or a turbulence model is used. In the case of running the case with DNS the increment of size should be smaller than if a RANS model is applied.

#### 3.2.1.2 Tangent discretisation

When settling the tangent discretisation in the boundary layer, it is important to have in mind the aspect ratio of the cells since $\Delta y_1$ has the smallest height. As general rule, aspect ratio in the boundary layer should be below 1:40.

After some tests, it has been noticed that using that maximum aspect ratio has influenced negatively in the appearance of vortex shedding. As result of the tests, it has been used a maximum relation of 1:14 in the extrados and maintained 1:40 in intrados, since vortex shedding are wanted to be as defined as possible.

As vortexes are expected to appear in extrados, the tangent discretisation on this zone has higher density than in intrados. In the Figure 3.4 it can be seen that the cells in extrados tend to be squared in order to capture the developed vortexes, whilst in intrados cells are wider. This time, the tangent growth rate has been used so that the change of aspect ratio is smooth.

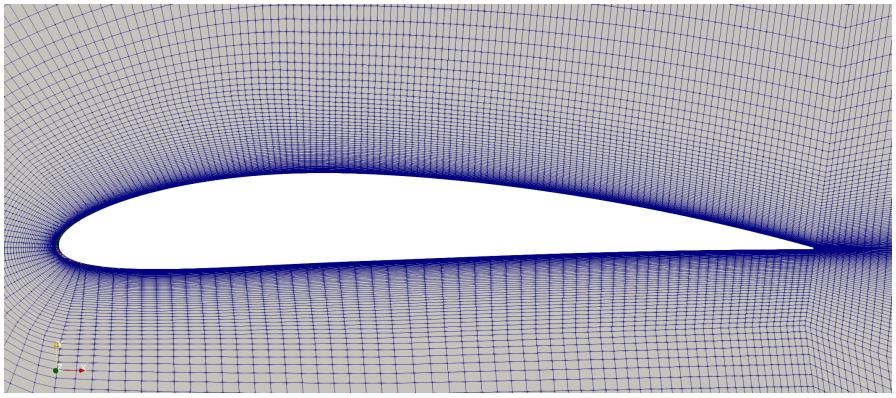

FIGURE 3.4: Boundary layer mesh.

### 3.2.2 Far field mesh

The starting point to build the far field mesh is the last cell of the boundary layer mesh. The far field includes the upstream, upper and lower regions of the airfoil.

The tangent discretisation of the boundary layer has to be maintained in the far field, whereas, the normal discretisation growth rate can be modified. Indeed, as it is not expected to find important changes on fluid direction, it is recommended to increase the growth rate up to 10-15% in order to reduce the number of cells.

As specified in the domain geometry, the wake region has its own face. The number of segments on the vertical discretisation is given by the normal discretisation of the boundary layer.

The growth scale could be modified on the right side, in order to obtain the distribution desired. This region should be dense just after the airfoil in order to catch properly the wake. For this reason, it has been used a horizontal discetisation which increments gradually when moving away from the airfoil.

The resulting 2D mesh is the one represented in the Figure 3.5. The outstanding mesh density on the upper and lower sides of the airfoil is caused by the discretisation on the boundary layer and on the trailing edge.

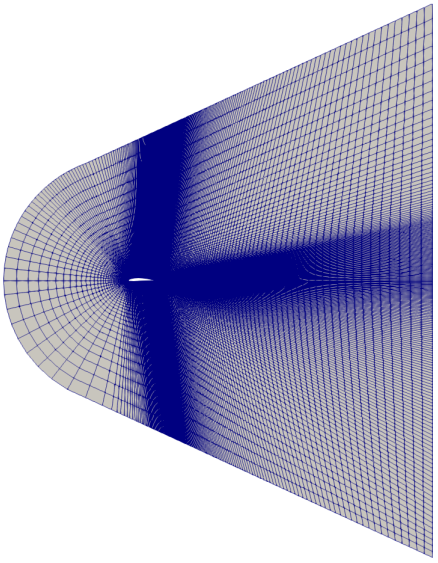

FIGURE 3.5: Domain Mesh.

On the contrary, the mesh density on the downstream zone on the airfoil is made intentionally to capture the vortex shedding. Furthermore, it is slightly moved upwards as the detached flow is predicted to move in that direction.

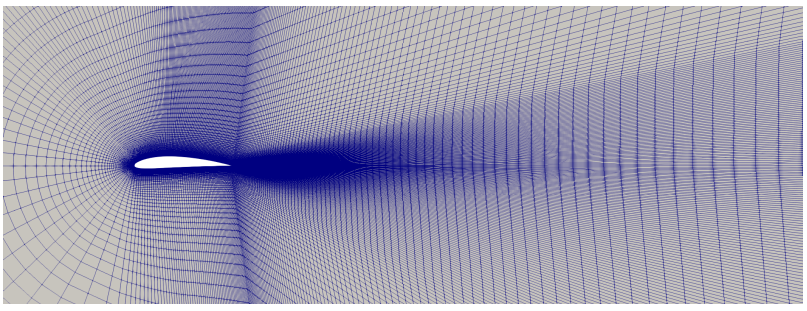

FIGURE 3.6: Downstream dens mesh.

## 3.3 Extrusion

As explained before, at this point the mesh has to be extruded one cell in Z-direction in order to obtain the finite volumes.

Before executing the extrusion it is needed to pre-select the group of edges that are defined as boundary conditions to identify later the so called patches in OpenFOAM.

These patches include the inlet, outlet and the airfoil walls. It has to be noted that the airfoil patches have been defined as intrados and extrados separately because it is of interest for the later result extraction. Moreover, it is also needed to select the faces of each cell to later on be defined as front and back patches, which will be empty of physical meaning as no flow changes will be computed in the Z-direction.

The last step is to create a compound mesh joining all the meshed regions. Then, the extrusion can finally be carried out. The extrusion length has been 5% of the chord, in order to prevent high 3D aspect ratio.

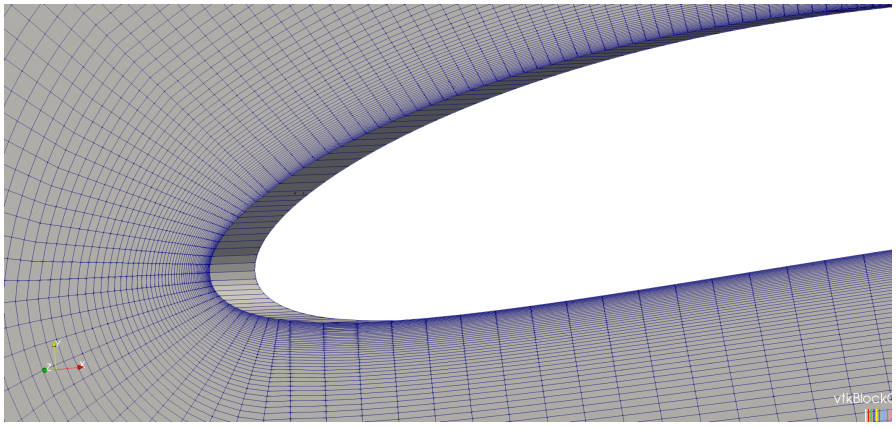

FIGURE 3.7: 3D mesh in leading edge

After the extrusion the mesh is ready to be exported and used for the CFD solving. The exportable mesh will be an *.unv* file that will be later converted to an OpenFOAM mesh.

## 3.4 Mesh quality

The quality of the mesh is evaluated with parameters that assure there will not be significant errors of calculation that would enlarge the convergence of the result due to the shape of the cells. The main parameters evaluated are the aspect ratio, the non-orthogonality and the skewness of the cells. [11] [12]

### 3.4.1 Aspect ratio

As commented before, the aspect ratio is a parameter to have in mind during the mesh generation. The face aspect ratio is the relation between the longest and the shortest length. But it can also be evaluated the cell aspect ratio, which is the ratio between the biggest and the smallest areas of the cell's bounding box. According to [12], having high aspect ratios would decrease the convergence speed.

### 3.4.2 Non-orthogonality ratio

This parameter measures the angle between the line connecting two cell centres and the normal of their common face. Having high values of this angle could be prejudicial. When the mesh is in OpenFOAM, with the command `checkMesh` one can find the maximum and the average values of the mesh evaluated. For instance, for the mesh with $y^+$=1 the output is shown in Listing 3.1.

```
Mesh non-orthogonality Max: 45.8741 average: 17.7234 \\
non-orthogonality check OK.
```

Listing 3.1: Non-orthogonality checkMesh.

The OpenFOAM documentation recommends to have less than 70 degrees of non-orthogonality. When this value is exceeded, after `checkMesh` command, it is written a file containing the bad faces. It is important to be below 70 in order to avoid nonOrthoCorrectors, which would imply an increment of iterations and thus, more time of computation. It should never be near 90.

### 3.4.3 Skewness ratio

This parameter is related to the non-orthogonality and aspect ratio since it measure the distance between the intersection of the line connecting two cell centres with their common face and the centre of that face. The smaller the parameter the better in accuracy results. It should never exceed 20.

This parameter can be analysed with the Salome 9 interface or the checkMesh utility. With the same mesh as before, the output of the `checkMesh` is the next

```
Max skewness = 2.10074 OK.
```

LISTING 3.2: Skewness checkMesh.

# Chapter 4

# OpenFOAM Setup

In the current Chapter it is going to be carried out the preparation of the OpenFOAM case in order to solve the fluid properties for a given problem. The Chapter will be structured following the disposition of directories and files that are needed to run the case.

## 4.1 OpenFOAM solver used

The case that is going to be solved is considered incompressible for its low Mach number (<0.3). As the study is focused on the boundary layer and a high AoA is used (10º) the viscous effects are important, and therefore the turbulence has to be computed.

For the study that is developed it is mandatory to consider the transient effects; first, in the detachment of boundary layer and after, in the effects of the Active Flow Control.

Hence, the case is treated as incompressible and transient, with turbulence modelling. For this type of flow OpenFOAM has two main solvers, a part from the solvers focused on specific cases. These two main solvers are pisoFoam and pimpleFoam. PisoFoam will be preferred, as pimpleFoam is addressed to unstable cases, it works following a similar procedure as pisoFoam, but with a higher number of verifications in the calculations.

Having defined the flow properties, the case can be prepared. As explained in the Chapter 1 the OpenFOAM folder contains three main directories, these are time directory, constant and system.

## 4.2 Time directory

The time directory is named after the time of the field properties that it contains, for example 10 for t=10. It is usually set as 0, if not previous solutions are used.

The time directory is necessary for the initial conditions of the solution, these initial conditions have to be defined for the pressure and velocity fields. Also, using the Spalart-Allmaras turbulence model, the initial fields for the turbulent kinematic viscosity and the modified viscosity have also to be specified.

### 4.2.1 Velocity field

The initial and boundary conditions of the boundary field are specified in the U file.

The file is composed by three main entries. First, the dimensions, which are defined as a vector, after the uniform or nonuniform velocity for the internal field and finally, the conditions that must be satisfied at the boundaries.

The dimensions are defined in a vector where the second position is distance [m] and the third is time [s], and the values of the vector are the exponent of the units. The result is shown in the Listing 4.1.

```
dimensions [0 1 -1 0 0 0 0];
```

Listing 4.1: Velocity dimensions.

The internal field velocity must be specified by its components. As the airfoil has been positioned with an angle of 0º and the domain has been designed allowing different angles of inlet velocity, the 10º AoA has to be created with the inlet velocity.

With a velocity of 4.5m/s and an AoA of 10º, the resulting components of the velocity are the ones shown in the Listing 4.2.

```
internalField uniform (4.431634889 0.7814167995 0.);
```

Listing 4.2: Velocity internal field components.

The boundaries of the case are the inlet and outlet of the domain, the walls of the airfoil and the front and back faces due to the mesh extrusion. These boundaries are defined in the polyMesh folder, which is explained on the Section 4.3.1.

- **inlet and outlet**

The velocity on the inlet will be the same as the internal field, while at the outlet is defined as zero gradient, meaning that it will remain constant. These are written as the Listing 4.3 shows.

```
    outlet
    {
        type zeroGradient;
    }
    inlet
    {
        type fixedValue;
    value     uniform (4.431634889 0.7814167995 0.);
    }
```

Listing 4.3: Velocity boundary conditions of inlet and outlet.

- **front and back**

For the front and back boundaries the entry type has been set as empty, in order to deactivate the solving in the z-direction. The corresponding entry is shown in the Listing 4.4.

```
    frontAndBack
    {
            type empty;
        }
```

LISTING 4.4: Velocity boundary conditions of front and back.

- **airfoil walls**

Finally, the velocity on the airfoil boundaries, which are divided in extrados and intrados for post-process purposes, will be set 0, as the velocity on the surface will be always zero. The Listing 4.5 shows these boundaries.

```
        intrados
        {
            type fixedValue;
        value    uniform (0. 0. 0.);
        }
        extrados
        {
            type fixedValue;
        value    uniform (0. 0. 0.);
        }
```

LISTING 4.5: Velocity boundary conditions of airfoil walls.

### 4.2.2 Pressure field

The pressure field is specified in the p file inside the time directory and has the same entries as the velocity file.

The dimensions of kinematic pressure are $[Pa/kg/m^3]$ which specified in the previously mentioned dimensions vector are $[m^2/s^2]$. The result is shown on the Listing 4.6.

```
dimensions [0 2 -2 0 0 0 0];
```

LISTING 4.6: Kinematic pressure dimensions.

As the pressure field will be computed with relative pressure, the internal field value of pressure is 0, as shown on the Listing 4.7.

```
internalField uniform 0.;
```

Listing 4.7: Kinematic pressure internal field value.

The boundary conditions of pressure are the following.

- **inlet and outlet**

The same as velocity happens for the pressure, the inlet value is the same as the internal field and the outlet is set to zero gradient. This is shown in the Listing 4.8.

```
    outlet
        {
            type fixedValue;
        value uniform 0.;
        }
    inlet
        {
            type zeroGradient;
        }
```

Listing 4.8: Pressure boundary conditions of inlet and outlet.

- **front and back**

Also for the front and back boundaries the entry type has been set.

- **airfoil walls**

Finally, the pressure on the airfoil boundaries has been set to zero gradient, this can be seen in the Listing 4.9.

```
    intrados
        {
            type zeroGradient;
        }
    extrados
        {
            type zeroGradient;
        }
```

Listing 4.9: Pressure boundary conditions of airfoil walls.

### 4.2.3 Turbulent kinematic viscosity

The turbulent kinematic viscosity field is specified in the nut file inside the time directory. The dimensions of the $\nu_t$ are $[m^2/s]$ resulting in the Listing 4.10.

```
dimensions      [0 2 -1 0 0 0 0];
```

LISTING 4.10: Turbulent kinematic viscosity dimensions.

The turbulent kinematic viscosity internal field has a value which is almost 0 following the reference [7], for this reason it has been set to 0. This is shown on the Listing 4.11.

```
internalField   uniform 0;
```

LISTING 4.11: Turbulent kinematic viscosity internal field value.

The boundary conditions of $\nu_t$ have been defined following the reference [7].

- **airfoil walls, inlet and outlet**

The value of the turbulent kinematic viscosity on the walls is 0, as well as on the inlet and outlet, as it is stated on the reference. These are shown in the Listing 4.12.

```
    intrados
        {
            type            nutLowReWallFunction;
            value           uniform 0;
        }
    extrados
        {
            type            nutLowReWallFunction;
            value           uniform 0;
        }
    outlet
        {
            type            calculated;
            value           uniform 0;
        }

    inlet
        {
            type            calculated;
            value           uniform 0;
```

LISTING 4.12: Turbulent kinematic viscosity boundary conditions of the airfoil walls, inlet and outlet.

- **front and back**

Again, empty is the entry for the front and back boundaries.

### 4.2.4 Spalart-Allmaras modified viscosity

The Spalart-Allmaras modified viscosity field is specified in the nuTilda file inside the time directory.

The dimensions of the $\nu$' are $[m^2/s]$. Thus, the vector results in the Listing 4.13.

```
dimensions      [0 2 -1 0 0 0 0];
```

Listing 4.13: Spalart-Allmaras viscosity dimensions.

The internal field value is also extracted from [7] and it has a null value, as shown on the Listing 4.14.

```
internalField   uniform 0;
```

Listing 4.14: Turbulent kinematic viscosity internal field value.

The boundary conditions of $\nu_t$ have been defined following the reference [7] and are the following.

- **inlet and outlet**

The Spalart-Allmaras modified viscosity field on the inlet and outlet boundaries has a value between 3 and 5 times the freestream kinematic viscosity, which for the case is $\nu_\infty = 1.805 \times 10^{-5}$. The resultant $\nu$' is shown in the Listing 4.15.

```
    outlet
    {
        type            freestream;
        freestreamValue uniform 0.00000542;
    }
    inlet
    {
        type            freestream;
        freestreamValue uniform 0.00000542;
    }
```

Listing 4.15: Turbulent kinematic viscosity boundary conditions of inlet and outlet.

- **front and back**

The front and back boundaries entry is still empty.

- **airfoil walls**

On the walls the $\nu$' is set to 0, this can be seen in the Listing 4.16.

```
    intrados
    {
        type            fixedValue;
        value           uniform 1e-20;
    }
    extrados
    {
        type            fixedValue;
        value           uniform 1e-20;
    }
```

LISTING 4.16: Turbulent kinematic viscosity boundary conditions of airfoil walls.

## 4.3 Constant

The constant directory contains files that define the mesh as well as files in which the thermophysical and turbulence settings are specified.

### 4.3.1 polyMesh folder

The polyMesh folder contains all the information about the mesh. The files composing it are:

- **faces**, file where all the mesh faces are defined.
- **neighbour**, list of neighbour cells for each face.
- **owner**, list of owner cells for each face
- **points**, list of coordinates describing the cell vertices.
- **boundary**, list of patches with the faces composing each patch, this file will be explained as it is crucial for the simulation.

#### 4.3.1.1 Boundary file

It is of high importance to define correctly the boundaries or patches of the case, in order to assign the boundary conditions, which are essential for solving the case.

In the case of study four types of boundary conditions are used; inlet, outlet, wall and empty. These have to be carefully specified with the number of cells that are composing it. The assignation of the number of cells to the boundaries has been done with Salome and after the OpenFOAM entries have been defined.

The empty type is used for 2D simulations that have to be extruded in order to obtain the finite volumes, but the flow will no have variations in the 3rd direction. The cells assigned to this patch are the front and back ones, as shown on the Listing 4.17.

```
frontAndBack
{
    type            empty;
    nFaces          77516;
    startFace       77107;
}
```

Listing 4.17: Front and back boundaries.

The wall type is for the solids, in this case the airfoil patches. In the Listing 4.18 this assignation can be seen together with the cells composing the patches.

```
intrados
{
    type            wall;
    nFaces          80;
    startFace       154623;
}
extrados
{
    type            wall;
    nFaces          136;
    startFace       154703;
}
```

Listing 4.18: Airfoil boundaries.

The inlet and outlet are entered as a patch type, this one does not contain geometric nor topological information about the mesh. These are shown on the Listing 4.19.

```
    outlet
    {
        type            patch;
        nFaces          196;
        startFace       154839;
    }
    inlet
    {
        type            patch;
        nFaces          406;
        startFace       155035;
    }
```

LISTING 4.19: Inlet and outlet boundaries.

The Active Flow Control boundary assignation will be explained on the Section 6.3.

### 4.3.2 Turbulence properties

As explained on the Chapter 2, Section 2.2.1 the case will be solved with Reynolds-Averaged Simulation modelling, so the simulation type has to be specified as RAS. Being selected the type, some entries are required regarding the turbulence modelling.

These, as shown in the Listing 4.20, are the turbulence model that will be used, which as explained in the Section 2.2.1 will be the Spalart-Allmaras, and the turn on of the computing of turbulence and the print of the coefficients at the start of the simulation.

```
simulationType RAS;

RAS
{
    RASModel        SpalartAllmaras;

    turbulence      on;

    printCoeffs     on;
}
```

LISTING 4.20: Turbulence modelling of the case.

In the case that more detailed results of the turbulence are wanted, with higher definition on the vortexes, the simulation could be solved with Direct Numerical Simulation. If DNS is used, the simulation type should be written as laminar, without turbulence modelling.

### 4.3.3 Transport properties

In the transport properties file the values and units of density $\rho$ and kinematic viscosity $\nu$ are specified. Also, the $\nu$ modelling is required, the model used is the Newtonian model which considers that $\nu$ is constant. These specifications are shown in the Listing 4.31

```
transportModel  Newtonian;

rho             [1 -3 0 0 0 0 0] 1.225;

nu              [0 2 -1 0 0 0 0] 0.00001805;
```

LISTING 4.21: Transport properties of the case.

## 4.4 System

Is the folder where the setting parameters of how the solution is performed are specified, giving the user a high control on the solving procedure.

The essential files in the system folder are 3: controlDict where run control parameters are set; fvSchemes where discretisation schemes are defined; and, fvSolution where the equation solvers, tolerances and algorithm controls are set.

### 4.4.1 Control Dictionary

The controlDict is the file where the time and writing settings are placed, it is also where functions can be added in order to obtain the results wanted.

The first thing needed to be specified in the solver that will be used, in the current case pisoFoam as determined at the begging of the Chapter, Section 4.1. This is shown in the Listing 4.22.

```
application     pisoFoam;
```

LISTING 4.22: Specification of the OpenFOAM solver that will be used.

Afterwards, the time settings have to be indicated. The computation time at which the solution will start, the computation time at which it will finish and the time step that will be computed from the start time until the end time. These settings have to be carefully chosen and some tests have to be run before the final set, as each case will have different convergence time and time step limit.

Nevertheless the time step needed for a determined case conditions can be approximated.

#### 4.4.1.1 Time step

It is mandatory that the time step is sufficiently small in order to catch the variations of the flow in time, otherwise the calculations done would not represent the real flow behaviour. This limit of time step depends both on the velocity and on the cell size, as at least the time that it takes the flow to travel between two cells has to be computed.

There is a condition relating these three parameters in order to find a the limit time step that can not be exceeded, this condition is a dimensionless number, the *Courant – Friedrichs – Lewy* number, which is calculated as shown on the equation (4.1).

$$C = \frac{u_x \Delta t}{\Delta x} + \frac{u_y \Delta t}{\Delta y} \leq 1 \tag{4.1}$$

being $u_x$ and $u_y$ the velocities in each direction, $\Delta t$ the time step and $\Delta y$ and $\Delta x$ the cell sizes.

As the velocities are not known at every point, the time step will be calculated by running tests, as the *Courant* number can be shown during the simulation to see if it exceeds 1. When the number goes beyond this value the simulation diverges quickly and it crashes. After a trial and error process the required time step for each simulation has been found.

The time settings displayed in the Listing 4.23 are the ones for the mesh with an $y^+ = 0.8$.

```
startFrom       latestTime;

stopAt          endTime;

endTime         15;

deltaT          0.0000095;
```

LISTING 4.23: Time settings of the ControlDict file for the $y^+$

After the time control settings, the writing settings are needed to be specified. The ones selected are shown on the Listing 4.24.

```
startFrom       latestTime;

stopAt          endTime;

endTime         15;

deltaT          0.0000095;

writeControl    timeStep;

writeInterval   2500;

purgeWrite      0;

writeFormat     ascii;

writePrecision  6;
```

LISTING 4.24: Writing settings of the ControlDict file

As mentioned before, functions are added at the end of the control directory in order to extract results.

Firstly, the residuals function has been added in order to save the residuals at each time step and see the convergence of the results. This is done as exposed in the Listing 4.25.

```
#includeFunc residuals
```

LISTING 4.25: Residuals function.

Afterwards, the function of the aerodynamic coefficients is written and some parameters need to be specified. It is important to define correctly the patches at which these coefficients are calculated, in this case are the airfoil ones. It is also required to define the Lift and Drag forces direction, which will be aligned with the free-stream flow. Finally, it is also important to define correctly the reference length (the chord of the airfoil) and the reference area (the chord multiplied by the extrusion length).

The resulting force coefficients function is shown on the Listing 4.26.

```
forces
   {
       type            forceCoeffs;
       libs ( "libforces.so" );
       patches         ("extrados" "intrados");
       rhoInf          1.225;
       liftDir         (-0.1736481777 0.984807753 0);
       dragDir         (0.984807753 0.1736481777 0);
       CofR            (0.05 0 0);
       pitchAxis       (0 0 1);
       magUInf         4.5;
       lRef            0.2;
       Aref            0.002;
   }
```

LISTING 4.26: Aerodynamic coefficients function.

Another function has been added in order to make sure that the $Y^+$ intended on the creation of the meshes is the real one. The recalculation is due to the flat plate approximation used when calculating the first cell size, see Sections 3.2.1.1 and 5.1. The function implementation is represented in the Listing 4.27.

```
  yPlus1
      {
         type         yPlus;
         libs         ("libfieldFunctionObjects.so");
         writeControl   timeStep;
         writeInterval  2500;
}
```

LISTING 4.27: $y^+$ calculation function.

The last function that has been added is the wall shear stress function which is needed for the calculation of the friction coefficient, in order to find the separation point of the boundary layer. The function is shown in the Listing 4.28.

```
   wallShearStress1
      {
          type         wallShearStress;
          libs         ("libfieldFunctionObjects.so");
          patches          ("extrados" "intrados" );
          writeControl   timeStep;
          writeInterval  2500;
     }
```

LISTING 4.28: Wall shear stresses calculation function.

### 4.4.2 Numerical Schemes

In the file fvSchemes the numerical schemes for the calculations done during the solving process are specified. In the Listing 4.29 the schemes for each term are defined, these terms are the time derivatives, gradients, divergence, laplacian, interpolation, etc. The selection of the schemes has been following the OpenFOAM page [13].

```
ddtSchemes
{
    default         CrankNicolson 0.5;
}

gradSchemes
{
    default         Gauss linear;
}

divSchemes
{
    default         none;
    div(phi,U)      Gauss limitedLinearV 1;
    div(phi,k)      Gauss limitedLinear 1;
    div(phi,epsilon) Gauss limitedLinear 1;
    div(phi,omega)  Gauss limitedLinear 1;
    div(phi,R)      Gauss limitedLinear 1;
    div(R)          Gauss linear;
    div(phi,nuTilda) Gauss limitedLinear 1;
    div((nuEff*dev2(T(grad(U))))) Gauss linear;
}

laplacianSchemes
{
    default         Gauss linear corrected;
}

interpolationSchemes
{
    default         linear;
}

snGradSchemes
{
    default         corrected;
}
wallDist
{
    method  meshWave;
}
```

Listing 4.29: Numerical schemes of the case.

### 4.4.3 Numerical Solution

In the fvSolution the solvers and algorithms to resolve determined equations are specified, also the tolerances are limited for different parameters. As the case will be solved with pisoFoam the PISO entry is required, with the number of correctors desired. All these can be found in the Listing 4.30

```
solvers
{
    p
    {
        solver          GAMG;
        tolerance       1e-06;
        relTol          0.1;
        smoother        GaussSeidel;
    }

    pFinal
    {
        $p;
        tolerance       1e-06;
        relTol          0;
    }

    "(U|nuTilda)"
    {
        solver          smoothSolver;
        smoother        GaussSeidel;
        tolerance       1e-05;
        relTol          0;
    }
}

PISO
{
    nCorrectors     2;
    nNonOrthogonalCorrectors 0;
    pRefCell        0;
    pRefValue       0;
}
```

Listing 4.30: Solvers, algorithms and tolerances used in the solution.

### 4.4.4 Parallelisation

The decomposeParDict file is needed if the case is wanted to be parallelised.

In this dictionary is where the number of cores used for the parallelisation is defined, as it will be the number of sub-processes in which the case will be divided. The domain is discretised by the simple method which consist in dividing it by directions, these divisions are chosen in the simpleCoeffs entry "n". Each number on the vector indicates the divisions on that direction, this is why the multiplication of the numbers in the vector must result in the number of subdomains specified previously.

```
numberOfSubdomains 20;

method          simple;


simpleCoeffs
```

Listing 4.31: Parallelisation of the case.

# Chapter 5

# Mesh Convergence and Baseline Case Results

The aim of this chapter is to select the optimal mesh in terms of computational cost and results accuracy. The four candidates which will have different $y^+$ and number of cells are going to be defined. It will be explained how to approximate the $y^+$ of the case and calculate the first cell height. In order to select the best mesh, a comparison between the results will be made for the same conditions.

Apart from that, further results obtained are going to be presented. The aerodynamic coefficients response over time will be displayed and their mean values will be calculated. Moreover, the pressure coefficient on intrados and extrados will be plotted for the four candidate meshes.

## 5.1 Mesh candidates definition

The four meshes presented have different height for the first cell and thus, in order to achieve the distribution presented in chapter 3, different number of cells. The $y^+$ chosen in order to achieve the mesh convergence are 1, 0.8, 0.5 and 0.3.

The first cell height can be calculated with equation 3.1. It is first needed to find the friction velocity and thus, the friction coefficient. Both parameters are defined as follows,

$$u_\tau = \sqrt{\frac{\tau}{\rho}}, \qquad \tau = \frac{C_f \rho V_\infty^2}{2} \tag{5.1}$$

It is common to use the friction coefficient from the flat plate as an approximation,

$$C_f = \frac{0.026}{Re^{1/7}} \tag{5.2}$$

It has to be noted that even if the first cell height does not correspond to the $y^+$ used, the mesh convergence will identify which $\Delta y$ is best. After running the simulation, it will be possible to find the real $y^+$ for each mesh as the friction coefficient will be known. At this point, it is possible to calculate $\Delta y$ with the physic properties of the case already set in Chapter 2 ($\rho = 1.225 kg/m^3$, $\mu = 1.805 \times 10^{-5} kg/ms$, $V_\infty = 4.5 m/s$ and $Re = 6.108 \times 10^4$).

In the Table 5.1, it is presented a summary of the main parameters that define the mesh. Values of non-orthogonality and skewness refer to the maximum values encountered considering all the cells in the domain, and the aspect ratio corresponds to the maximum value in the extrados of the boundary layer.

| $y^+$ | $\Delta y_1 \times 10^{-5}[m]$ | Nº of Cells | non-Orthogonality | Skewness | Aspect Ratio |
|---|---|---|---|---|---|
| 1.0 | 6.31 | 37,340 | 45.8741º | 2.10074 | 13.9 |
| 0.8 | 5.05 | 38,758 | 46.2615º | 2.10661 | 17.4 |
| 0.5 | 3.16 | 40,982 | 46.9812º | 2.11655 | 27.5 |
| 0.3 | 1.90 | 44,518 | 48.0075º | 2.13088 | 40.6 |

TABLE 5.1: Mesh candidates characteristics.

It can be seen that the number of cells increase as the $y^+$ decreases. The maximum values of non-orthogonality and skewness do not change significantly with $y^+$ changes while maximum aspect ratio on the extrados boundary layer increases considerably. This is because it has been intended to maintain the same distribution of cells in the boundary layer.

In the Figure 5.1 can be seen the four mesh candidates.

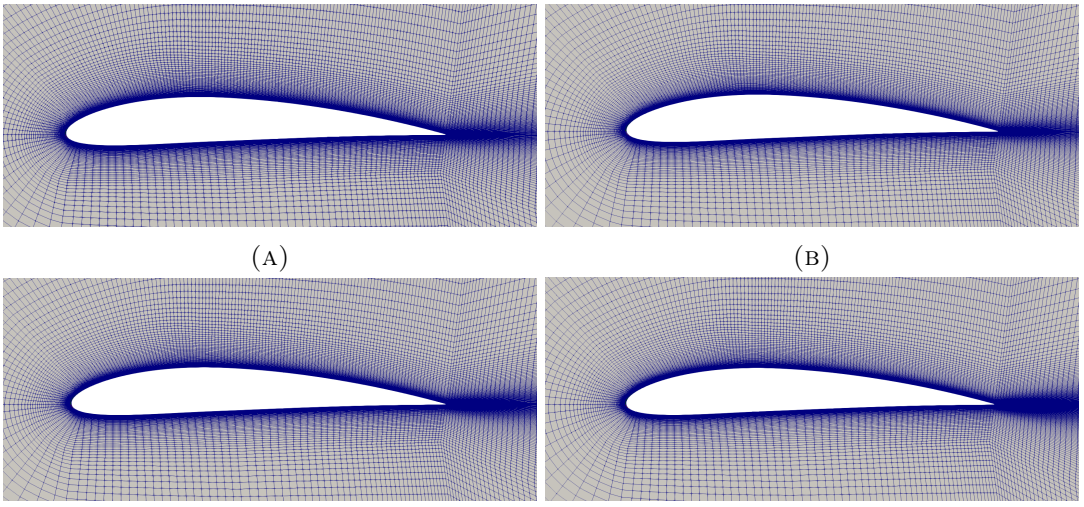

(A) (B)

(C) (D)

FIGURE 5.1: Meshes: (a) $y^+ = 1$, (b) $y^+ = 0.8$, (a) $y^+ = 0.5$ and (b) $y^+ = 0.3$.

It can be noted the similarity of the cell distribution in all the meshes and the density change due to smaller $\Delta y_1$, specially in the trailing edge.

## 5.2 Mesh results

Each mesh has been simulated for 15 computational seconds, or 337.5 non-dimensional time units using freestream velocity and the chord. If it is wanted to achieve high level of accuracy, it is recommended to enlarge this time until 100 computational seconds or more, since it exists the possibility of finding changes after that time. In the current study, due to the limited time and high computational cost of extending more time the solution, 15 seconds have been considered enough.

In the case of $y^+ = 5$, the simulation has been extended until 26 computational seconds in order to find out if the results change significantly. The difference that has been found between the mean values of lift coefficient is of 0.08% considering and not considering the last 10 seconds. Therefore, the solution of running 15 computational seconds has been accepted having into account the increase of time that running 10 computational seconds more implies.

Figures in 5.2 are the transient lift coefficients obtained for the different meshes along the non-dimensional time.

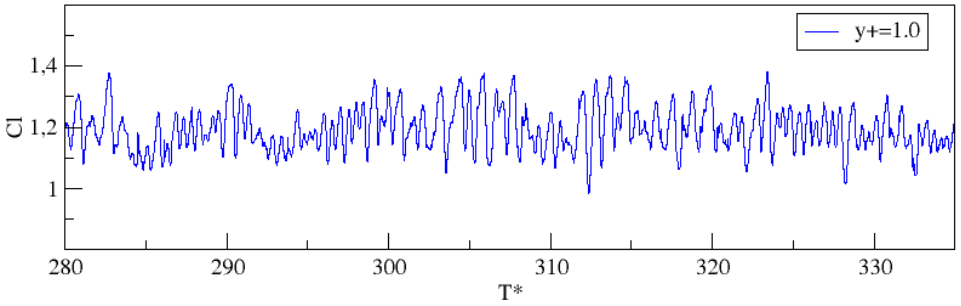


(A)

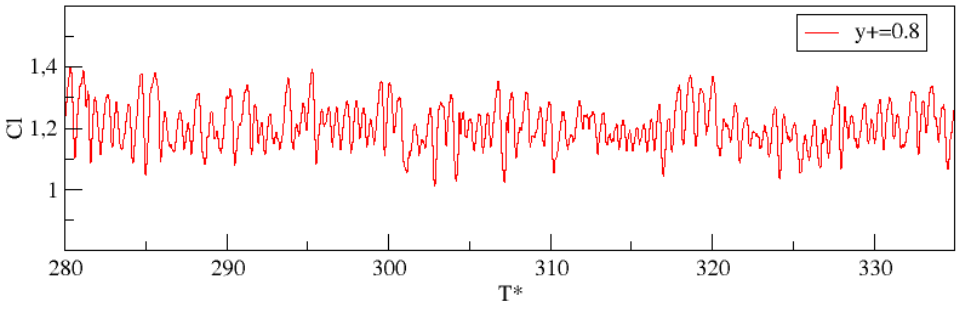


(B)

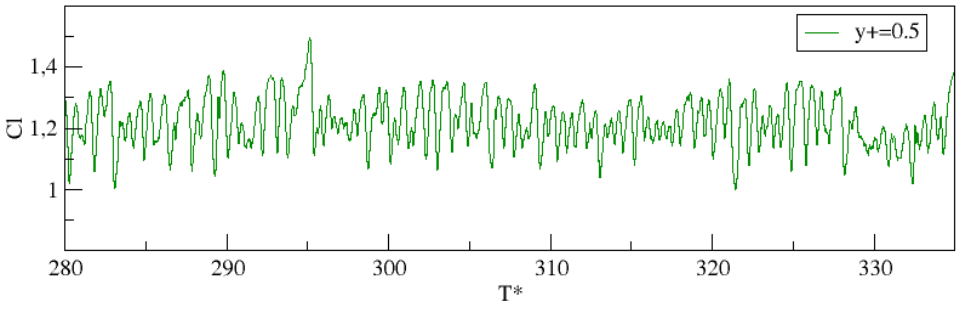


(C)

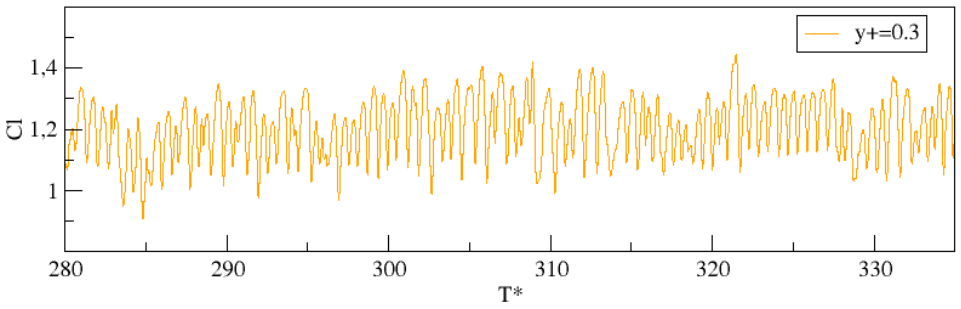


(D)

FIGURE 5.2: Transient lift coefficient for different $y^+$.

Figures 5.3 are the transient drag coefficients obtained for the different meshes along the non-dimensional time.

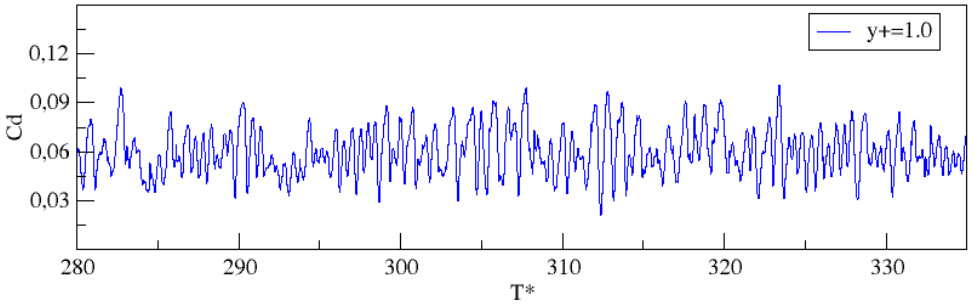


(A)

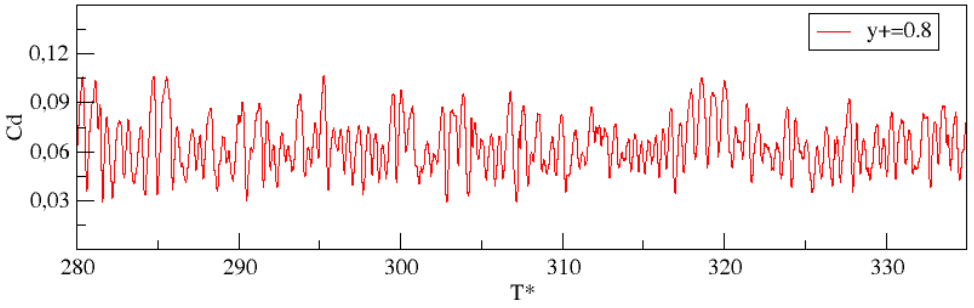


(B)

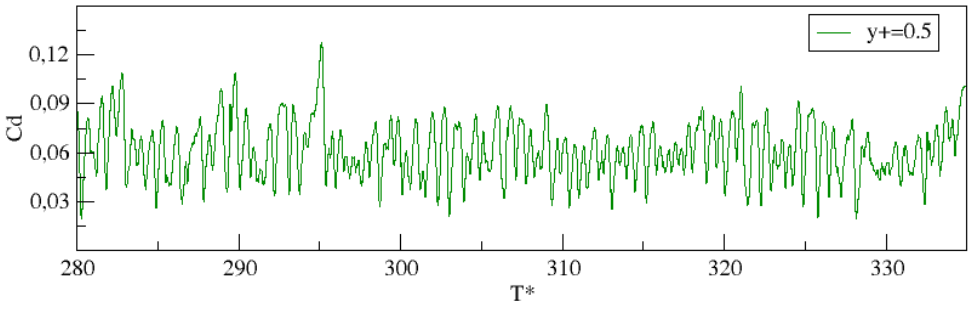


(C)

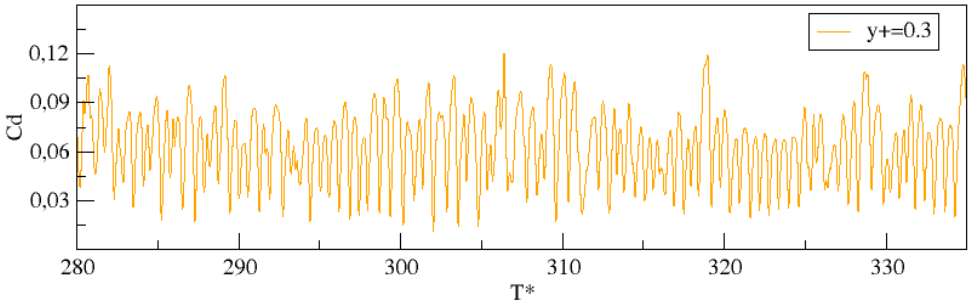


(D)

FIGURE 5.3: Transient drag coefficient for different $y^+$.

On the Figures 5.2 and 5.3 can be clearly seen the oscillations of the aerodynamic coefficients. As the case of study has a Reynolds number of $Re = 6.108 \times 10^4$, it was expected to find a noisy oscillation graph. When the Reynolds number decreases to $\times 10^3$, oscillations can be seen clearly and with less amplitude. This difference is caused mainly for the increment of turbulent flow. The amplitude of the oscillation is related to the size of the vortex shedding produced, therefore, when applying AFC, it is expected to reduce both the amplitude and vortex size.

Furthermore, the residuals of each iteration have been saved: Ux, Uy and first p (explained in Chapter 4). This values can confirm the convergence of the result if constant oscillation is found. In the Figure 5.4 the residuals of velocity for the $y^+ = 0.8$ mesh are presented.

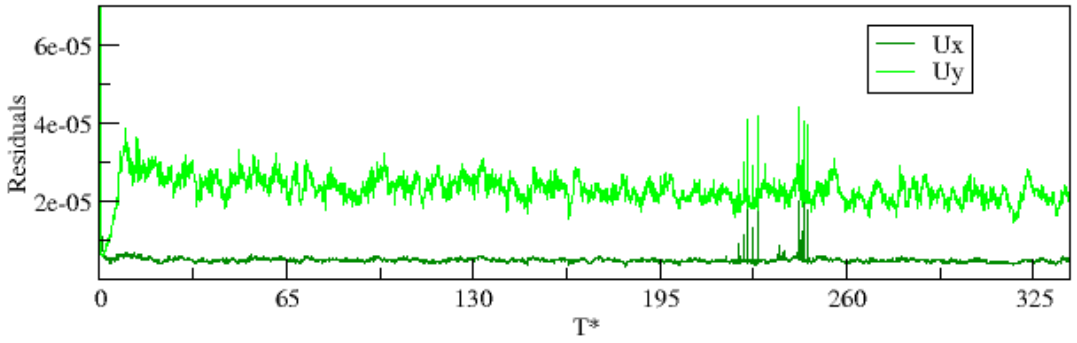


FIGURE 5.4: Ux and Uy residuals of $y^+ = 0.8$ mesh.

It can be seen that the Uy has a higher mean value and oscillates more than Ux. This might be because vertical velocity change more than horizontal velocity along time. It is recommended to have all residuals in the order of $\times 10^{-5}$ or less.

In order to obtain the optimal mesh, the mean values of the aerodynamic force coefficients have to be evaluated. These values have been calculated after removing the first 7 seconds, when the solution has already turned stable, considering stable, an error of 3% change of mean values. In the Table 5.2, the mean values of efficiency, lift and drag coefficients are presented.

| $y^+$ | $\Delta y_1 \times 10^{-5}[m]$ | Cl | Cd | E |
|---|---|---|---|---|
| 1 | 6.31 | 1.2111 | 0.0617 | 19.629 |
| 0.8 | 5.05 | 1.2100 | 0.0624 | 19.391 |
| 0.5 | 3.16 | 1.2079 | 0.0605 | 19.965 |
| 0.3 | 1.90 | 1.2084 | 0.0611 | 19.777 |

TABLE 5.2: Mean values of Cl, Cd and E of candidate meshes.

As it can be seen on the Table 5.2, the values obtained are notably close to each other, the maximum difference of lift coefficients are 0.26% while 3.04% for drag coefficients. If lower $y^+$ had been used, more accuracy could have been found. Nevertheless, the difference between $y^+ = 0.5$ and 0.3 have been 0.04% and 0.98% for lift and drag coefficients, respectively, which is a remarkable result.

In order to select which mesh it is going to be used for the further study, the computational time has been evaluated. In the Table 5.3 it is presented the computational cost of time for each $y^+$ and its respectives time steps. In the Table it has also been represented the real $y^+$ used for each $\Delta y_1$, meaning that the real friction coefficient has been applied.

| Approximated $y^+$ | Real extrados $y^+$ | Total time running [h] | Time step $\times 10^{-6}$ [s] |
|---|---|---|---|
| 1.0 | 0.5076 | 42 | 10.0 |
| 0.8 | 0.4003 | 45 | 9.5 |
| 0.5 | 0.2522 | 74 | 6.0 |
| 0.3 | 0.1771 | 105 | 4.0 |

TABLE 5.3: Mesh candidates characteristics II.

The real $y^+$ has resulted to be smaller than the approximated. Apart from that, it was obvious to find an increment of the running time when using a smaller $y^+$, not only because of the larger number of cells but also because of the time step used. As explained in Chapter 4, Courant number may never exceed the unit, thus, it has been used different time steps for each mesh due to the different cell sizes. It should be noted that the running time is for 15 computational seconds, run in parallel with 20 cores.

It is of interest to obtain the pressure coefficient along the chord. This graph is usually used to compare CFD results with experimental data. In this case, the pressure coefficient has been validated by comparing the result for the four meshes.

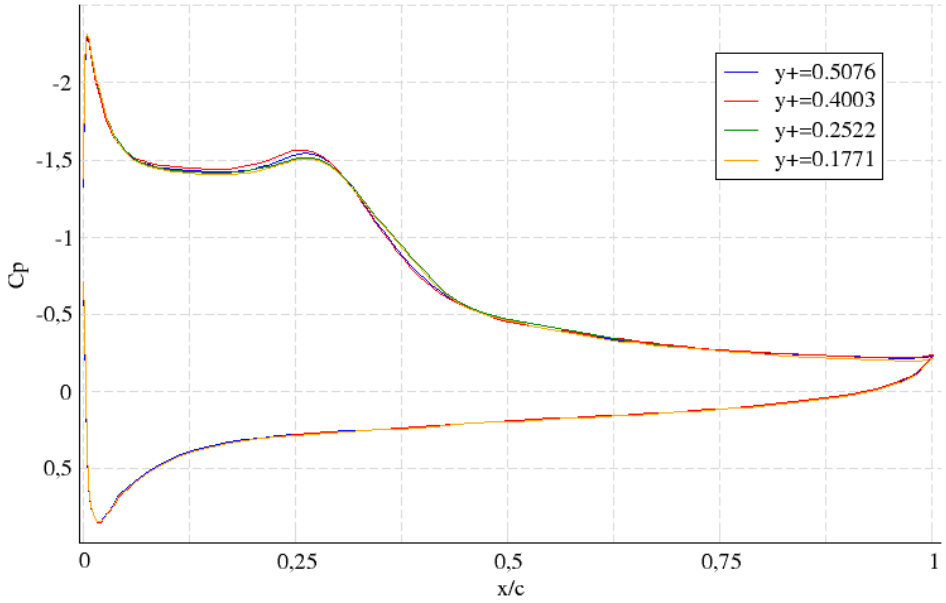


FIGURE 5.5: Pressure coefficient comparison.

As it is seen on the Figure 5.5 that the different discretisations have obtained a similar shape of Cp. In intrados results can not be distinguished between diferent $y+$, whereas in the extrados there are slightly differences. Regarding to the values obtained, it can be noticed an uncommonly shape of Cp in extrados compared to a fully attached flow over an airfoil.

The abrupt fall of the Cp at the leading edge means the layer separation due to the formation of the laminar bubble. The maximum located just after 25% of the chord is located the transition of point, it where flow changes from laminar to turbulent. The next abrupt fall denotes the reattachment, which in this case, it is not possible to locate it clearly. The Cp could be compared with the in-viscid solution in order to recognize better those points. In Figure 5.6, it is shown the velocity field. The blue spot in the extrados before the flow detaches, is the laminar bubble, characteristic for medium thickness airfoil (see Chapter 2).

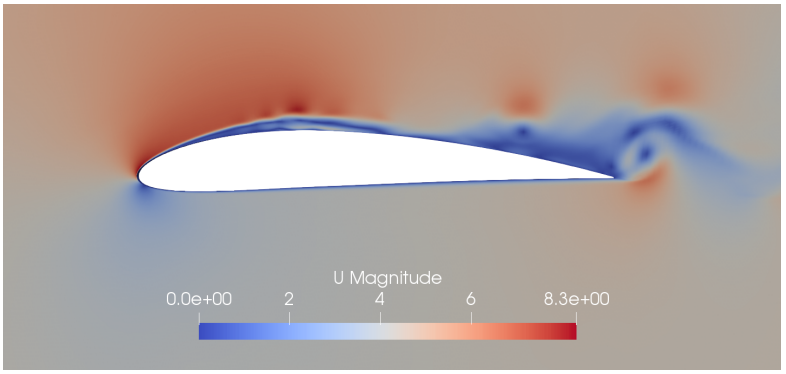


FIGURE 5.6: Velocity field in [m/s] of the Baseline case at T*= 312.

In order to locate more precisely the separation point it has been used another method of higher accuracy, presented in the Chapter 6.

All things considered, it has been chosen the mesh of $y^+ = 5$ to continue the study, since it has an acceptable accuracy level for this level of research, error of 0.04% in lift and 0.9% in drag compared to the finer mesh. It can be seen in Figure 5.3, the considerable less time consuming when obtaining results, which is of major importance in a short time study. The mesh with $y^+ = 3$, needs 30% more time than $y^+ = 5$, being this fact the determinant.

# Chapter 6

# Active Flow Control Implementation

The aim of this chapter is to process the Baseline case results in order to obtain the active flow control features. This includes its placement and geometry, and the jet input signal of velocity. For this reason, it will be presented the new mesh and the implementation of the jet in OpenFOAM.

In Chapter 5, it has been confirmed the appearance of the laminar bubble on extrados. Although it has been possible to estimate the localization of the detachment, it is needed more accuracy in order to select where to place the slot of the AFC. For this reason, it will be calculated the friction coefficient along the chord in order to find the exact point where shear stress is null, and thus, where the flow detaches.

Active flow Control can be used in different ways as Chapter 1 has introduced. This Thesis is focused in fluidic control, and more concretely, in zero-net-mass-flux. To implement ZNMF it is needed to create an oscillating signal of velocity respect time. It will be presented how to calculate the signal for a given momentum coefficient and the implementation of the signal in the boundary conditions of OpenFOAM.

## 6.1 AFC features

According to different articles, such as [14] [2], it is essential to place the pulsating jet near the separation point. Therefore, the first step to apply the active flow control mechanism is to find the location where it has to be placed. After, it is needed to calculate the input signal and define which angle of blowing will have with respect to the normal.

### 6.1.1 AFC placement

From the articles before mentioned, the tendency is to locate the slot before boundary layer detaches. Recommended values for these parameters should be used as initial guess, afterwards, it would be needed to try different positions in order to find the optimum slot localization and width. In the current study, the optimization of the last two parameters will be considered out of the scope and will remain constant for the whole test.

In order to find the separation point, it has been plotted the friction coefficient along the chord and found the first root of the function obtained. OpenFOAM does not provide directly the friction coefficient, so the data has been processed with paraView and it has been followed the next procedure. First of all, it has been extracted the time in which the simulation is converged following the same criteria used in Chapter 5. Afterwards, it has to be done a time average of the wall shear stresses computed in the extrados, the result is shown in Figure 6.1.

FIGURE 6.1: Average wall shear stress distribution on extrados of Baseline case.

It has to be noted that it is needed the average values because shear stresses change in time. Indeed, it is known from the theory explained in Chapter 1 that during a transient case, the separation point oscillates and due to the oscillation, it is produced the vortex shedding along extrados. This mean value of shear stress would indicate the center points from where the values oscillate.

Besides, it is also needed to extract the normal surfaces of the extrados in order to calculate the shear stress projection into the tangents of the surface. As last step, it is required to make the tangent wall shear stress non-dimensional with freestream velocity, density and the characteristic length. The resultant plot can be seen in Figure 6.2.

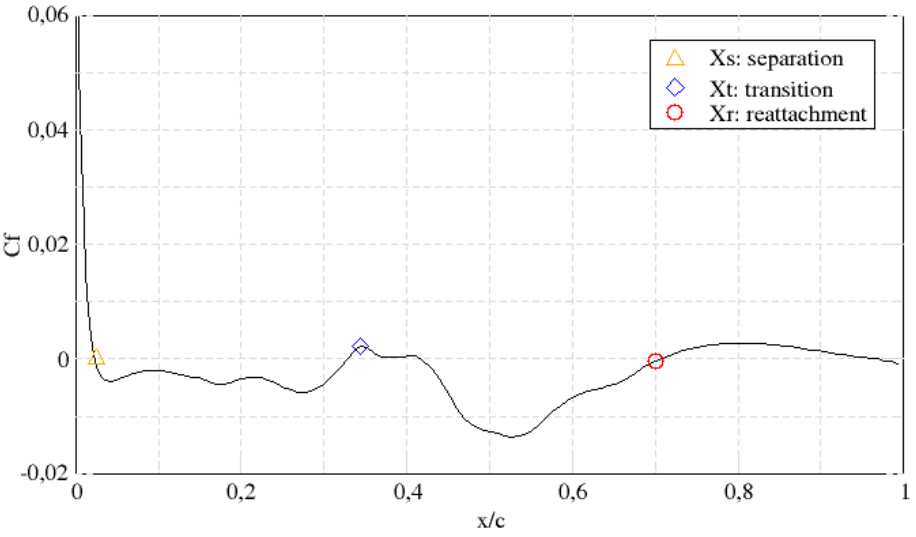


FIGURE 6.2: Friction coefficient of Baseline case.

Due to the high AoA used in the case, it has been found the first separation point $X_s = 4.826$ mm at 2.4% of the chord, notably close to the leading edge. This plot can explain clearly the physics behind the problem. Negative sign on friction coefficient means that the shear stresses in the wall are acting opposite direction to the x coordinate and thus, the flow too.

From $X_s$ to $X_t$, it is placed the laminar bubble since the change of sign indicates the change of circulation in the wall. $X_t$ is the transition point from laminar to turbulent flow. In Figure 6.3, it can be seen that the vortex bubble may rotate clockwise. Just in the $X_t$, it is generated a little vortex which rotates counterclockwise, it can be seen in Figure 6.3. This little vortex does not commonly appear for lower Reynolds number.

After the bubble, when the friction coefficient turns positive again, the reattachment happens. From $X_t$ to $X_r$, it is generated a clockwise vortex with higher intensity than the laminar bubble.

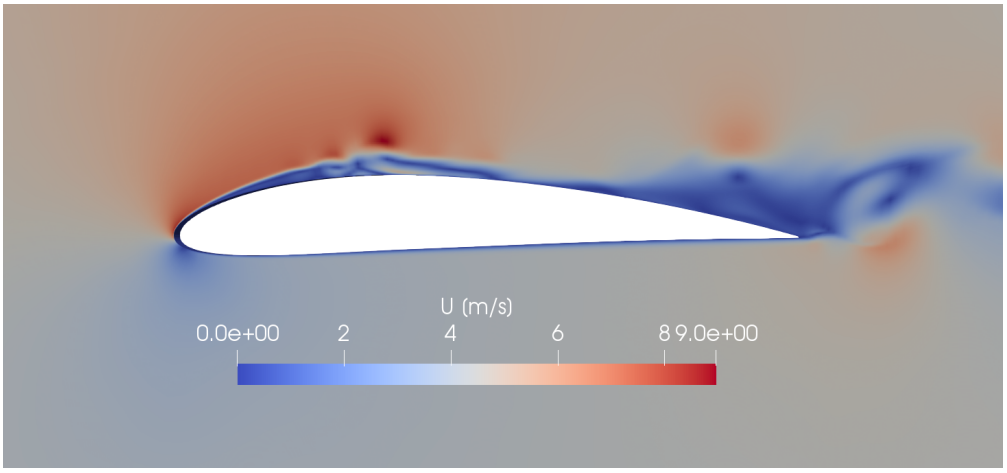


FIGURE 6.3: Velocity field at T*= 320.

As the separation point has been found very near to the leading edge the slot end will be located at the position $X_{slot} = 3.426$ mm, 0.7% before the detach point, and it will have a width of 2 mm.

In section 6.2, it is going to be explained how the slot has been implemented in the mesh.

### 6.1.2 AFC input velocity signal

The present study focuses on the implementation of the zero-net-mass-flux actuator. Therefore, as explained in section 1.2, the aim is to produce a sinusoidal velocity signal.

In order to generate that signal it is needed to define a certain amplitude and a oscillation frequency. It should be noted that these values will be found and used as initial guess. In Chapter 7, it is developed a comparison of different values of amplitude and frequency to find the optimum configuration.

The signal wanted will be ruled by Equation 6.1.

$$u_{jet}(t) = A\sin(2\pi ft) \tag{6.1}$$

If periodic forcing is wanted to be applied, the additional mass would be provided by including a constant to the signal.

#### 6.1.2.1 Amplitude

The amplitude is related to the velocity blown and the velocity is studied with the momentum coefficient.

The momentum coefficient gives a relation between the jet and freestream velocities and is defined as Equation 6.2 states.

$$C_\mu = \frac{\rho_{jet}\bar{u}_{jet}^2 w}{\frac{1}{2}\rho_\infty V_\infty^2 c} = 2\frac{w}{c}\left(\frac{\bar{u}_{jet}}{V_\infty}\right)^2 \tag{6.2}$$

At this point, it can be obtained the velocity of the jet by settling the momentum coefficient into a certain value. According to [14] [2], a common value of this coefficient is 0.002, so the comparison of Chapter 7 will be made around this momentum coefficient.

Once the velocity of the jet is defined it can be found the amplitude by equalizing the momentum developed by the sinusoidal signal and the constant jet velocity in half period $T/2$. A graphical representation is exposed in Figure 6.4.

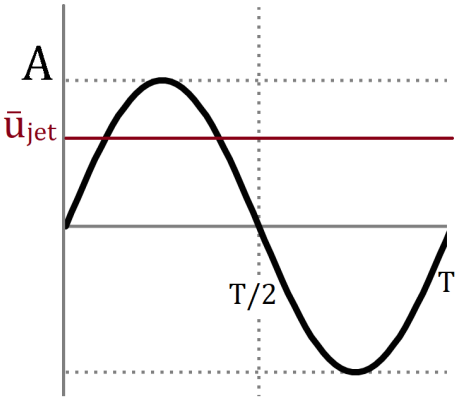


FIGURE 6.4: Velocity field at T*= 320.

It can be easily found the amplitude with Equation 6.3

$$A = \frac{\bar{u}_{jet}T}{2\int_0^{T/2} sin(\frac{2\pi}{T}t)dt} = \frac{\bar{u}_{jet}\pi}{2} \tag{6.3}$$

In the case of constant blowing or suction, the signal would be the constant with a value of mean jet velocity.

#### 6.1.2.2 Frequency

The intention of including a frequency in the signal is to stabilize somehow the turbulent frequency and reduce the size of vortex shedding generated in the extrados. Once again, this value has to be found by try and error if the optimal is wanted to be found. As an initial guess, it will be used the first frequency obtained of applying the Discrete Fourier Transform (DFT) to the lift coefficient signal as [14] recommend.

As turbulent flow generates a very noisy signal of aerodynamic coefficients, a clear value is difficult to be obtained. In this case, it has been used Xmgrace software in order to process the data.

In Figure 6.5, it is shown the frequencies obtained from doing the DFT to the lift coefficient of Figure 5.2b, since it has been the signal with a more clear first frequency.

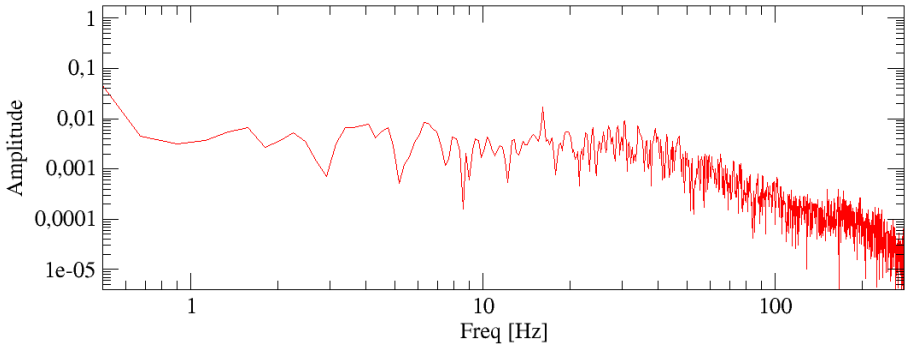


FIGURE 6.5: DFT of lift coefficient.

The first excitation frequency can be located at 16.3 Hz. This will be the reference frequency from which different tests will be performed in Chapter 7.

## 6.2 AFC Mesh

The purpose of this study is to simulate the effect of the active flow and not the actuator mechanism. For this reason, the mechanisms will be simplified into a slot placed on the surface of the airfoil.

As concluded in Chapter 5, it will be used the mesh with the $y^+ = 0.5$. The slot is located at $X_{slot} = 3.426$ mm, and this point belongs to the first extrados boundary layer face, as it can be seen in Figure 3.3. Therefore, the mesh will be only changed in two faces, the boundary and far field corresponded.

### 6.2.1 Geometry change

As explained in Chapter 3, it is necessary first to change the geometry. It has been spotted the coordinates of the airfoil spline with the $X_{slot}$ and the two points of the slot has been added to the geometry ($P1(0.003426, 0.005657)$ and $P2(0.001920, 0.004353)$).

Having in mind the boundary condition declaration, it is needed to generate separately the spline of the slot and the rest of airfoil. At this points, it has been done the same with the boundary layer and far field splines. In Figure 6.6 it can be seen the result.

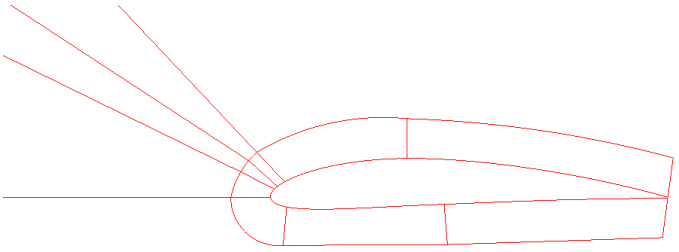

FIGURE 6.6: Geometry AFC implementation.

It has to be noted that the slot region had to be perpendicular to the surface in order to generate the mesh with the inlet direction, this angle is 130.89º.

### 6.2.2 Slot discretization

The discertization of the slot has to be finer than the rest of the mesh, it is recommended not to exceed an Aspect Ratio of 1:5. In this case, in order to fill the width of the slot, it has been used 21 segments, having an Aspect Ratio of 1:3. The result can be seen in Figure 6.7.

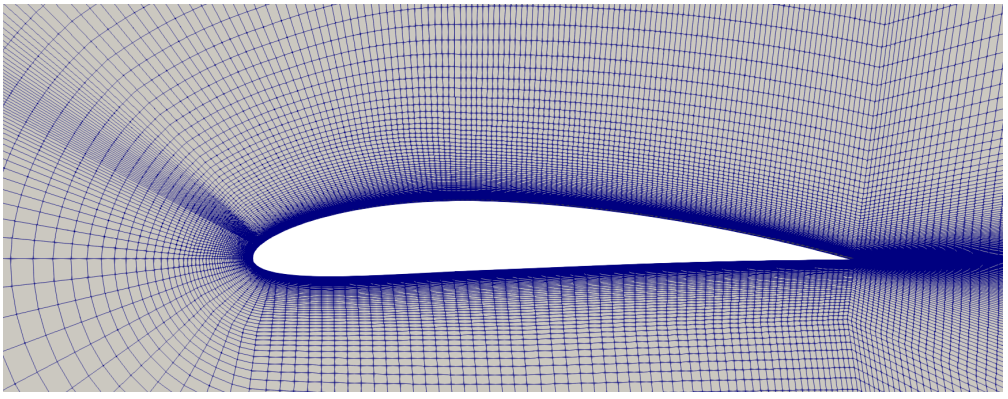

FIGURE 6.7: Mesh AFC implementation.

It can be seen that the sides of the slot mesh have been densified in order to have a smoother size transition. The augment of the number of cells can be seen in Table 6.1

| | Baseline case | AFC case |
|---|---|---|
| Nº of Cells | 40,982 | 43,989 |

TABLE 6.1: Number of cells comparison.

## 6.3 AFC setup in OpenFOAM

As it has been introduced a new boundary patch, it has to be included in the file boundary in /constant/polyMesh folder. Indeed, it has to be added also in all files of /0 folder which it has been defined with the same parameters as the inlet, unless the U file.

In the U file is where the inlet fuunction is going to be defined. For a momentum coeficient of 0.002 and the first frequency, the U file is defined as in the Listing 6.1.

```
AFC
    {
       type            uniformFixedValue;
           uniformValue    sine;
       uniformValueCoeffs
       {
           frequency    16.3;
           amplitude    2.2392;
           scale    (-0.6545864717 0.7559871368 0);
           level    (0 0 0);
       }
     }
```

LISTING 6.1: AFC boundary condition of velocity in OpenFOAM

It can be seen that the velocity has been defined as a sine with the respective frequency and amplitude. The scale parameter is an amplifier, in this case it has been used to set the angle of inlet. In the case of study, the velocity of the jet will be blown perpendicular to the surface, changing the blowing angle will not be considered in the comparison. The scale parameter is expressed as unit vector, in this case the angle is 130.89º. The level parameter represents the offset of the signal, as this example is for a ZMFA, this value is null.

If constant suction or constant blowing is implemented, it has to be defined as the inlet, uniform value with a certain angle.

# Chapter 7

# Active Flow Control Results

The aim of this Chapter is to compare different configurations of the AFC inlet velocity and discuss results obtained. As stated in Chapter 6, if it is wanted to fully optimize the performance of the airfoil with AFC, it is needed to do a study of the influence of each of the parameters that defines the mechanism. Nevertheless, the amplitude and the frequency of the signal will be the design variables, since the current study focuses on ZNMF.

In order to compare the results for different amplitude and frequency, it will be evaluated the mean values of lift and drag coefficient and the delaying of the separation point. During the comparison, baseline results will be included

## 7.1 AFC comparison

As the aim is to find the optimal case that improves the performance of the Baseline case: $C_l = 1.2079$, $C_d = 0.0605$ and E= 19.618. The amplitudes tested have been chosen from similar momentum coefficient order of magnitudes values used in [14] [15]. Regarding the frequencies, it has been tested multiples of the first excitation frequency.

Simulations has been run for 10 computational seconds, with the same hardware used in the Baseline case. As explained in Chapter 6, the time step has been reduced due to small size of the mesh in the slot region and therefore, computational cost has incremented.

### 7.1.1 Momentum coefficient test

The intention is to simulate the case for different momentum coefficient applied in the slot, in order to find the adequate $C_\mu$. As explained before in section 3.7, changing the momentum coefficient implies different amplitude signal and thus, different velocity blown and suctioned.

Results will be displayed in Figures 7.1 and 7.2 in order to observe the tendency of enhancement. Afterwards, the whole data will be summarized in Table 7.1 in a more detailed format.

Figure 7.1 shows the mean value of lift coefficient for each momentum coefficient. It has to be noted that it has been used the same procedure as before to obtain mean values.

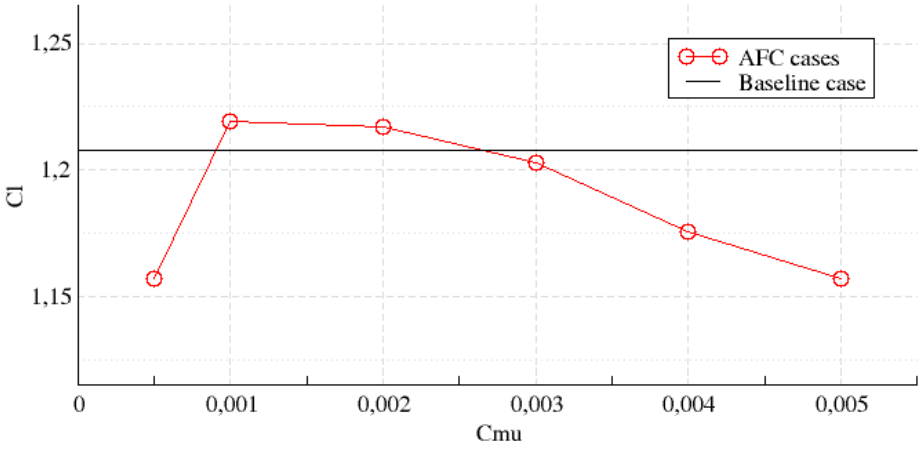


FIGURE 7.1: Lift coefficient for different momentum coefficient in AFC.

From this firsts results, it can be said that the values of lift coefficient are no improving considerably. There has been only two cases in which the coefficient has enhanced the Baseline case, $C_\mu = 0.001$ and 0.002.

Figure 7.2 shows the mean value of drag coefficient for each momentum coefficient.

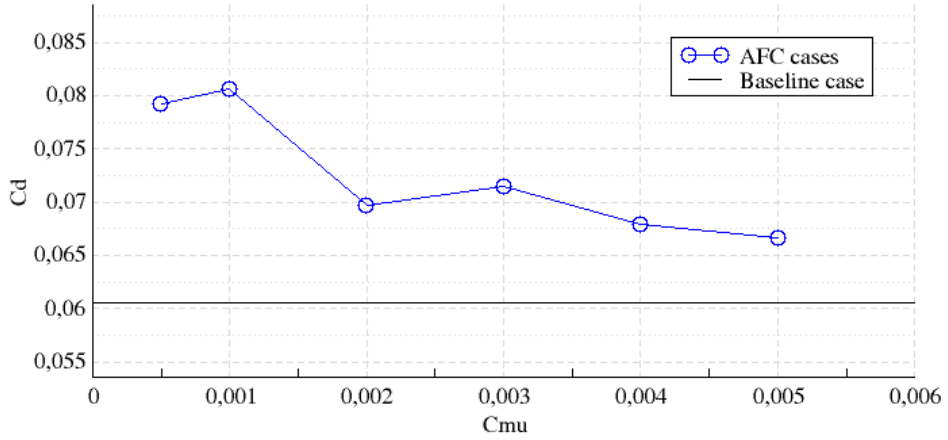


FIGURE 7.2: Drag coefficient for different momentum coefficient in AFC.

As can be seen in Figure 7.2, drag coefficient has not been improved in any of the cases tested. For lower momentum coefficient the drag coefficient increased considerable its value. It has been found a possible cause of this increment in drag in section 3.7.

In order to compare lift and drag coefficient together, it has been included Table 7.1. It has been evaluated the increment of lift coefficient and the decrement of drag coefficient with respect to the Baseline case. Moreover, it has been included the efficiency of each case.

| $C_\mu$ | 0.0005 | 0.001 | 0.002 | 0.003 | 0.004 | 0.005 |
|---|---|---|---|---|---|---|
| $+\Delta C_l$ [%] | -2.39 | **0.92** | 0.75 | -0.40 | -2.65 | -4.21 |
| $-\Delta C_d$ [%] | -30.91 | -33.22 | -15.12 | -18.1 | -12.23 | **-10.08** |
| E | 14.79 | 15.38 | **17.46** | 16.82 | 17.31 | 17.16 |

TABLE 7.1: Result summary of AFC for different $C_\mu$ with respect to Baseline case.

The best results obtained have been marked in bold. No single case has been found that stands out for its results compared to the others. However, cases of $C_\mu = 0.001$ and 0.002 have been chosen for continue the comparison with different frequencies, since both have improved the lift coefficient.

### 7.1.2 Frequency test

As seen on the previous section, the excitation frequency used has not demonstrated to be an exceptional frequency for the case. The magnitude of the frequencies are going to be changed in terms of non-dimensional frequency, defined as the frequency applied on the jet with respect to the frequency of the flow. Table 7.2, presents the frequencies that will be used.

| $F^+$ | F [Hz] | $C_\mu$ |
|---|---|---|
| 0.5 | 8 | 0.001 |
| 1 | 16.3 | 0.001 - 0.002 |
| 2 | 32 | 0.001 |
| 2.5 | 40 | 0.002 |
| 3 | 48 | 0.002 |
| 5 | 80 | 0.002 |

TABLE 7.2: AFC for different $F^+$.

It has to be noted that firstly, the values of $C_\mu = 0.001$ were tested, but after evaluating the results, the test of frequencies was changed to higher frequencies with $C_\mu = 0.002$.

Figure 7.3 shows the mean value of lift coefficient for each non-dimensional frequency.

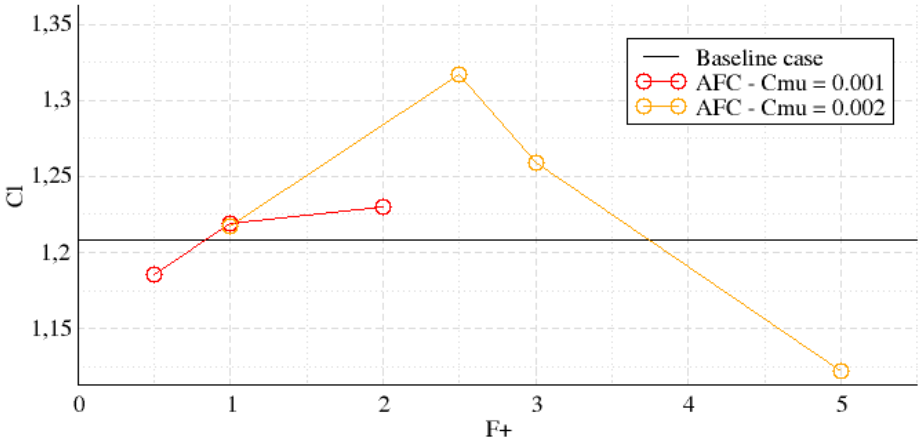


FIGURE 7.3: Lift coefficient for different frequency in AFC.

With the variation of frequency, it has been able to find three more cases that improve lift coefficient. Moreover, it has been found that the performance improves for about two times the non-dimensional frequency. It has to be noted that higher frequencies should have been studied for $C_\mu = 0.001$ and lower ones for $C_\mu = 0.002$, in order to make a complete comparison of the performance.

Figure 7.3 shows the mean value of drag coefficient for each non-dimensional frequency.

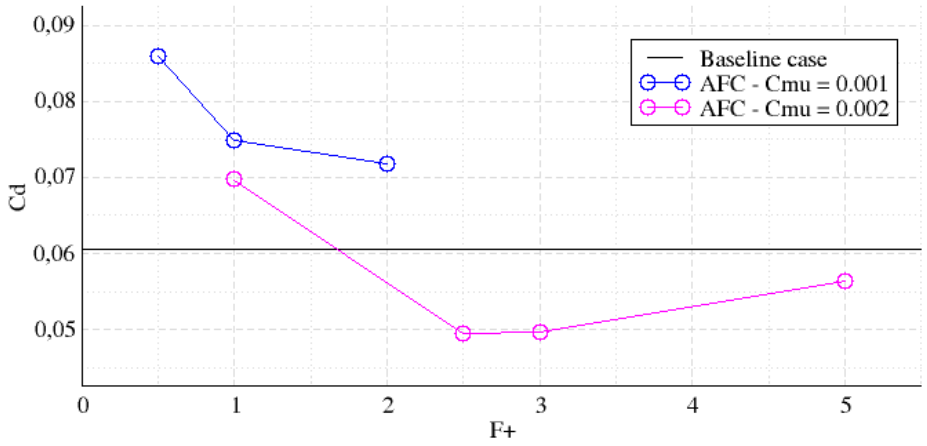


FIGURE 7.4: Drag coefficient for different frequency in AFC.

It has been found out that combinations of $C_\mu = 0.002$ and non-dimensional frequencies around 2.5 produce considerable efficiency improvements. Apart from that, drag coefficients obtained for $C_\mu = 0.001$ have finally been discarded as a good option, even tough lift coefficients improved.

| $C_\mu$ | 0.001 | | | 0.002 | | | |
|---|---|---|---|---|---|---|---|
| $F^+$ | 0.5 | 1 | 2 | 1 | 2.5 | 3 | 5 |
| $+\Delta C_l$ [%] | -1.83 | -0.92 | 1.846 | 0.75 | **9.00** | 4.21 | -7.10 |
| $-\Delta C_d$ [%] | -42.0 | -23.8 | -18.7 | -15.0 | **18.2** | 17.9 | 6.8 |
| E | 13.78 | 15.25 | 13.13 | 17.46 | **26.37** | 25.52 | 19.89 |

TABLE 7.3: Result summary of AFC for different frequency with respect to Baseline case.

As done before, best results are in bolt. It can be seen that there has been found two case that stand out from the others. Both cases has increased considerably the efficiency of the Baseline case, $E_{Baseline} = 19.618$. It can be said that for $C_\mu = 0.002$ and lower frequencies the efficiency decrements due to the high increment of drag. Further study could be done around $F^+ = 2.5$ and evaluate the sensitivity of the lift.

Further study on the physics behind the cases evaluated is explained in the next section.

## 7.2 Results evaluation

The aim of applying AFC in this case is to stabilize the transient boundary layer. From [16], it is possible to enhance the performance of an airfoil by changing the appearance of vortex along the chord. From the Baseline case, see Figure 3.7, it can be seen that after the laminar bubble the flow detaches, giving that a transition of big vortex along the airfoil. If AFC is properly implemented, the behaviour of the boundary layer can be changed into a generation of small vortex, attached to the airfoil, and in this way delaying the separation point. In that case, we would be expecting an improvement of the performance of the airfoil.

In this section is presented an evaluation of the pressure and friction coefficient for the best AFC case found and the Baseline case results, in order to understand the physics on the boundary layer.

Figure 7.5 shows the pressure coefficient of cases mentioned. It is expected to find a higher surface in the AFC case since the lift coefficient increased 9%.

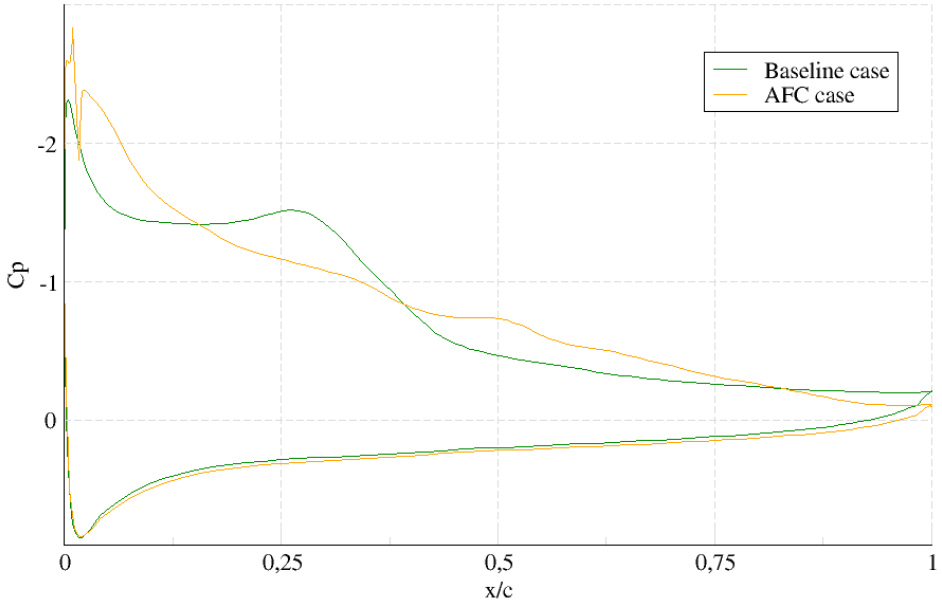


FIGURE 7.5: Pressure coefficient of Baseline and AFC case.

From Figure 7.5, it can be stated that there has been a change of shape and of surface. Regarding the Cp in extrados, it can be seen that the laminar bubble has disappeared in AFC case (see comments of Figure 5.5). However, the drop is not smooth, thus, that could indicate the presence of little vortexes. The described situation is in accordance with what has been described in the introduction of this section.

In order to deepen in the study, in Figure 7.6 is presented the friction coefficient of the Baseline and AFC cases.

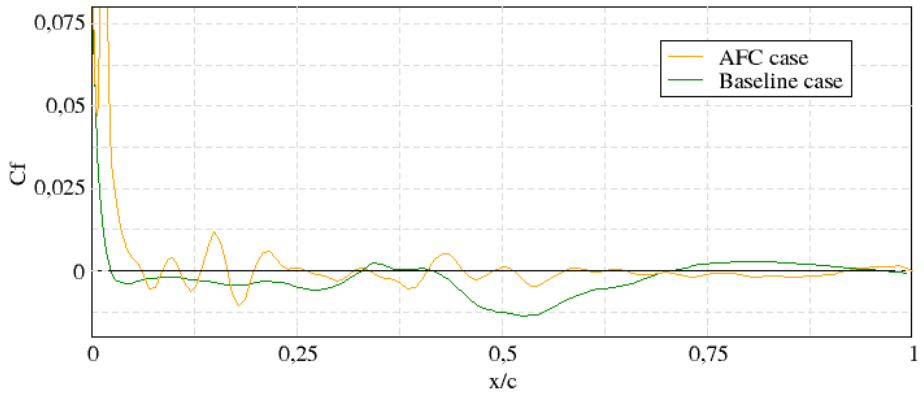


FIGURE 7.6: Friction coefficient of Baseline and AFC case.

With this result it can be confirmed the presence of small bubbles (see comments of Figure 6.2) after the AFC slot. It can be expected that the boundary layer is behaving as mentioned in the introduction since the friction coefficient might be indicating the presence of little vortex sliding on the extrados. To conclude this section, it is going to be displayed the velocity field of the AFC case in Figure 7.7,7.8 and 7.9.

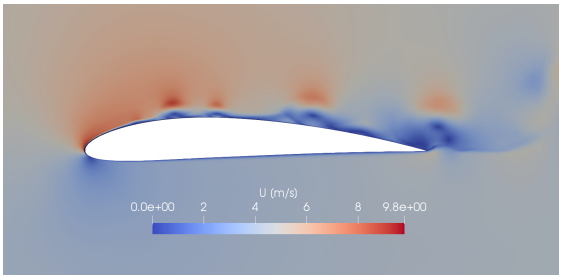


(A)

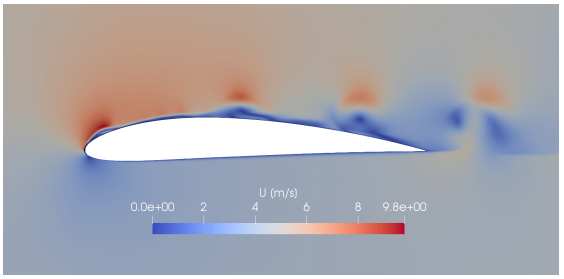


(B)

FIGURE 7.7: Transient velocity field in AFC case I.

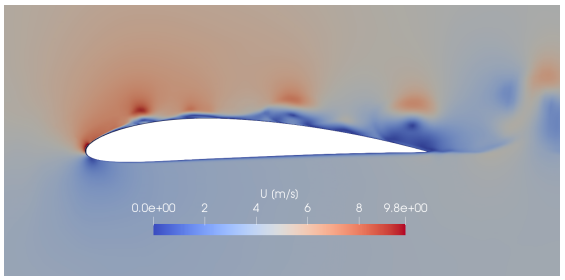


(A)

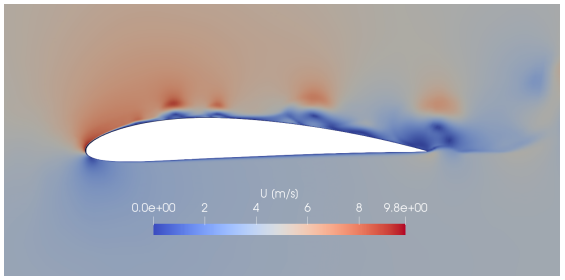


(B)

FIGURE 7.8: Transient velocity field in AFC case II.

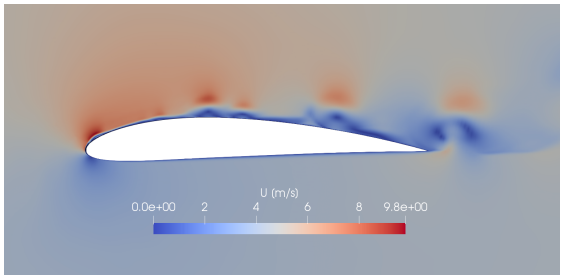


(A)

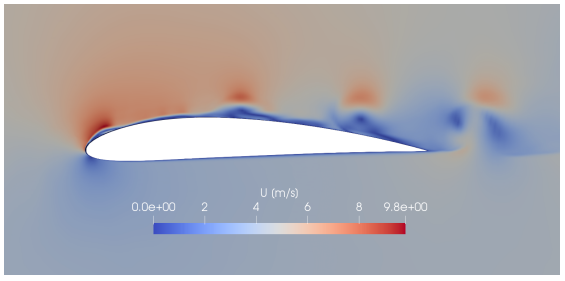


(B)

FIGURE 7.9: Transient velocity field in AFC case III.

# Chapter 8

# Conclusions

Regarding the to the aim of the study, it has been possible to evaluate the effect in the boundary layer and the performance of several cases actively controlled with ZNMF.

The methodology of resolution has been followed without eluding steps. It has been possible to acquire sufficient skills in mesh generations to produce a proper one. Nevertheless, it has to be noted, that this process took a long time, and it was required of some iterations. Finally, the mesh independence test has been successfully developed guaranteeing high accuracy in terms of mesh resolution and acceptable computational cost.

It has been found that the open-source OpenFOAM is fully prepared to solve a wide range of problems. There has been no problem in terms of shortage of information, on the contrary, thanks to the web support and the accessibility to forums, it is possible to solve high part of the problems encountered.

Regarding the Baseline results, it has been obtained results with physical meaning, and coherent respect to bibliography. The laminar bubble has been clearly obtained and intuited in friction and pressure coefficient. The four meshes generated obtained close results, however, it could have been evaluated a finer mesh to reassure the convergence of the mesh.

The AFC comparison has shown to be a slow process, since every case had to be run for minimum 7 days. For this reason, it has been only possible to evaluate the velocity and amplitude of the sinusoidal velocity signal of the jet. However, it has been found that with this two parameters the response can change considerable. It can be said that a lot of parameters are involved in the implementation of AFC, and the response is very

sensible to the change of them. Therefore, it can be a very large process to find the optimal solution for each case. Apart from that, the mechanism simplification has been very useful in terms of setting up the problem, since the mesh with the mechanism would have been very time consuming.

Regarding results of the AFC cases that improved the performance of the Baseline, it has been found as expected that in these cases, the coupling of the suction-blowing with the vortex frequency generates a sliding path on the extrados.

It has to be highlighted that this Thesis has been made in collaboration with the recognized research centre: International Centre for Numerical Methods in Engineering, providing access to a cluster for running the cases. Without doubt, this Thesis could not have been performed without the cluster. Even if there has been problems with the cluster, it has been accomplished the objectives of the Thesis thanks to the cluster.

Having spent four months of dedication to a single objective, it has to be said that from the starting point until now a lot of knowledge has been acquired in several fields discussed during the Thesis.

**Future Work**

As stated during the Thesis, there are a wide range of parameters that can be analyzed in an AFC mechanisms, such as dimensions of the slot, different placements etc. The consumed in the learning process have made it impossible to make a deep study considering all the variables affecting this mechanism. For this reason, many further developments can be made in a future work, having the present Thesis as a preliminary study.

The first improvement that should be done in a further study is the increase in the computational time computed of each result obtained, in order to reassure there are no changes in future iterations.

Another aspect that has to be studied is the accuracy of the Spallart-Allmaras turbulence model. A comparative analysis between different turbulence resolutions could be made in order to select the most fitted for the case, increasing the detail on the vortexes to achieve better accuracy in the AFC results, but without excessive computational time.

Finally, a more intense study should be done in the placement of the AFC on the airfoil and its width. This study should be done resolving more positions and sizes and making a comparison in order to obtain the best one. As it is a process of trial and error, it could also be done by an optimization process, trying as well as different geometry configurations, different frequencies of jet velocity and momentum coefficients.

# Bibliography


[1] https://m-selig.ae.illinois.edu/ads/coord_database.html.

[2] Melton, L. P., Schaeffler, N. W., Yao, C., and Seifert, A., "Active control of flow separation from supercritical airfoil leading-edge flap shoulder," *Journal of Aircraft*, vol. 42, no. 5, pp. 1142–1149, 2005.

[3] "NUMERICAL SIMULATION OF A SYNTHETIC JET ACTUATOR,"

[4] Graff, E., Seele, R., Lin, J., and Wygnanski, &. I., "Sweeping Jet Actuators-a New Design Tool for High Lift Generation," tech. rep.

[5] https://ntrs.nasa.gov/archive/nasa/casi.ntrs.nasa.gov/19930090976.pdf.

[6] Gul, M., Uzol, O., and Akmandor, I., "An experimental study on active flow control using synthetic jet actuators over s809 airfoil," in *Journal of Physics: Conference Series*, vol. 524, p. 012101, IOP Publishing, 2014.

[7] Modelling, N. T., "The spalart-allmaras turbulence model." https://turbmodels.larc.nasa.gov/spalart.html, 2019.

[8] Tang, L., "RANS Simulation of Low-Reynolds-Number Airfoil Aerodynamics," no. January, pp. 1–14, 2012.

[9] https://www.salome-platform.org/.

[10] http://airfoiltools.com/airfoil/details?airfoil=naca4415-il.

[11] https://openfoamwiki.net/index.php/CheckMesh.

[12] https://www.cfdsupport.com/OpenFOAM-Training-by-CFD-Support/node131.html.

[13] https://cfd.direct/openfoam/user-guide/.

[14] Tuck, A. and Soria, J., "Active flow control over a naca 0015 airfoil using a znmf jet," in *15th Australasian fluid mechanics conference*, pp. 13–17, 2004.

[15] Buchmann, N., Atkinson, C., and Soria, J., "Influence of znmf jet flow control on the spatio-temporal flow structure over a naca-0015 airfoil," *Experiments in Fluids*, vol. 54, p. 1, 03 2013.

[16] "Active Flow Control: A Review," tech. rep.

[17] https:https://turbmodels.larc.nasa.gov/spalart.html.

[18] Aftab, S. M. and Ahmad, K. A., "CFD study on NACA 4415 airfoil implementing spherical and sinusoidal Tubercle Leading Edge," *PLoS ONE*, vol. 12, aug 2017.

[19] Itsariyapinyo, P. and Sharma, R. N., "Large Eddy simulation of a NACA0015 circulation control airfoil using synthetic jets," *Aerospace Science and Technology*, vol. 82-83, pp. 545–556, nov 2018.

[20] Buchmann, N. A., Atkinson, C., and Soria, J., "Influence of ZNMF jet flow control on the spatio-temporal flow structure over a NACA-0015 airfoil," *Experiments in Fluids*, vol. 54, no. 3, 2013.

[21] Amzad Hossain, M., Nizam Uddin, M., Mustak, R., and Mashud, M., "Volume || 4 || Issue || 1 || Pages || PP," tech. rep., 2015.

[22] Mashud, M., Nizam Uddin, M., Waliullah, T., and Umemura, A., "\376\377\000M\000a\000s\000h\000u\000d\000-\0004\0007\000-\0005\0002," tech. rep., 2010.

[23] Aftab, S. M., Rafie, A. S., Razak, N. A., and Ahmad, K. A., "Turbulence model selection for low reynolds number flows," *PLoS ONE*, vol. 11, apr 2016.

[24] Munday, D., Jacob, J., Hauser, T., and Huang, G., "Experimental and Numerical Investigation ofAerodynamic Flow Control Using Oscillating Adaptive Surfaces," American Institute of Aeronautics and Astronautics (AIAA), dec 2012.

[25] Katam, V., "SIMULATION OF LOW-RE FLOW OVER A MODIFIED NACA 4415 AIRFOIL WITH OSCILLATING CAMBER," tech. rep., 2005.

[26] Shah, H., Mathew, S., and Lim, C. M., "Numerical simulation of flow over an airfoil for small wind turbines using the $\gamma$-Re $\theta$ model," *International Journal of Energy and Environmental Engineering*, vol. 6, pp. 419–429, dec 2015.

[27] Soria, J., Tuck, A., and Soria, J., "Active Flow Control over a NACA 0015 Airfoil using a ZNMF Jet Experimental techniques for the investigation of three-dimensional density fields in thermofluids View project Supersonic Twin Jet Coupling View project Active Flow Control over a NACA 0015 Air," tech. rep.

[28] Tran, S. A., Corson, D. A., and Sahni, O., "Synthetic Jet based Active Flow Control of Dynamic Stall Phenomenon on Wind Turbines Under Yaw Misalignment," American Institute of Aeronautics and Astronautics (AIAA), jan 2014.

[29] OMEARA, M. and MUELLER, T., "Experimental determination of the laminar separation bubble characteristics on an airfoil at low Reynolds numbers," American Institute of Aeronautics and Astronautics (AIAA), oct 2013.